Theoretical Analysis of E-J Characteristics and Evaluation of Pinning Potential in a Superconducting Bi-2223 Silver-Sheathed Tape

Takeshi Kodama

February, 2002

Information System Science

Contents

List of Figures

Chapter 1

Introduction

1.1 Introduction

In 1911 Kamerling Onnes discovered that the electric resistance of mercury had an unmeasurably small value when cooled to liquid helium temperature (4.2 K). Such a material was called superconductor. Since then, various superconductors have been discovered. In an early stage, pure metal and alloyed superconductors were developed, and the study of the superconductors was advanced. In 1957 the BCS theory was proposed to explain the mechanism of superconductivity. This theory predicted that the critical temperature at which the transition to the superconducting state takes place never exceeds 30 K. However, in 1986 Bednorz and Müller discovered a new superconductor which showed superconductivity at above 30 K.

Soon after that, various oxide superconductors with the critical temperatures above the boiling point of liquid nitrogen, 77 K, such as $YBa_2Cu_3O_x$, $Bi_2Sr_2CaCu_2O_x$, $Bi_2Sr_2Ca_2Cu_3O_x$ and so on, were discovered. An application of these high-temperature superconductors was desired to various fields because of economical merits. Especially, a cooling cost was expected to decrease, since the critical temperature of these oxide superconductors was higher than the boiling point of liquid nitrogen. However, in the past years, a difficulty of application of these superconductors was recognized, and nowadays not only a discovery of new superconductors with higher critical temperatures and an analysis of their structures, but also an improvement of superconducting properties necessary for application are required.

When considering an application of superconductors to various equip-

ments, it is necessary to quantitatively describe their transport characteristic (the current-voltage characteristic). Although the transport characteristic of metallic superconductors is fairly simple, that of high-temperature superconductors is quite difficult due to a strong thermal activation at high temperatures, a two-dimensional superconducting property owing to a crystal structure and so on. Especially, the critical current density decreases drastically at high temperatures due to the flux creep, as will be mentioned in section 1.2.2.

Therefore, it is necessary to clarify the flux pinning mechanism in order to improve the critical current density at high temperatures. For the purpose, a special theoretical analysis and a suitable measuring method are needed to describe the transport characteristic. Since the transport characteristic depends sensitively on the distribution of the pinning force, it is important to clarify the distribution. This will be helpful to clarify the mechanism of generation of the electric field in oxide superconductors.

1.2 Electromagnetic phenomena in high-temperature superconductors

Electromagnetic phenomena in high-temperature superconductors can also be fundamentally described by the Maxwell equations. In general, since the superconductor do not have a magnetization, we have $\boldsymbol{B} = \mu_0 \boldsymbol{H}$ between the magnetic field $\boldsymbol{H}$ and the flux density $\boldsymbol{B}$, where μ_0 is magnetic permeability of the vacuum. Therefore, hereinafter, we call $\boldsymbol{B}$ the magnetic field. The fundamental Maxwell equations are

$$\mathrm{rot}\boldsymbol{E} = -\frac{\partial \boldsymbol{B}}{\partial t}, \tag{1.1}$$

for the electromagnetic induction, and

$$\boldsymbol{J} = \frac{1}{\mu_0}\mathrm{rot}\boldsymbol{B} \tag{1.2}$$

for the current, where $\boldsymbol{E}$ and $\boldsymbol{J}$ are the electric field strength and the current density, respectively. Since the physical quantities are B, E and J, the equation related between E and J is needed in order to describe the electromagnetic phenomenon, except two equation as mentioned above, that is the

E-J characteristics. This represents the largest feature of the superconductor. This point is identical with metallic superconductors.

Note, Eq. (1.1) represents the generated electric field when the flux distribution changes in time, and such a variation is closely related to the flux motion. If the velocity of the flux lines is given by $\boldsymbol{v}$, during the variation of the flux distribution, we have

$$\mathrm{rot}(\boldsymbol{B} \times \boldsymbol{v}) = -\frac{\partial \boldsymbol{B}}{\partial t}. \tag{1.3}$$

This is called the equation of continuity of flux lines. Comparing Eq. (1.1) with Eq. (1.3), we have

$$\boldsymbol{E} = \boldsymbol{B} \times \boldsymbol{v}. \tag{1.4}$$

(Mathematically, we need to add a gradient of some scalar function to this equation. However, it is proved that the value is zero.) This is called the Josephson equation.

1.2.1 Critical state model

Even if the flux lines experience the Lorentz force by the current inside the superconductor, those are trapped due to the force of various defects such as dislocations, normal precipitates, voids and grain boundaries, and the electric field is not induced. This phenomenon is called the flux pinning. In this case we have only to consider the balance between the Lorentz force the flux lines experience and the pinning force which prevents their motion. This force balance, which gives a fundamental proof of the $\boldsymbol{E}$–$\boldsymbol{J}$ characteristics, is described by the critical state model.

When the flux lines pass near defects such as normal precipitates, the flux lines feel the variation of energy. This causes the flux pinning and the pinning force is given by the variation rate of the energy. The Lorentz force the flux lines experience per unit volume is given by $\boldsymbol{J} \times \boldsymbol{B}$. Since the pinning force density is in directed opposite to the Lorentz force, if an unit vector in the direction of the Lorentz force is $\boldsymbol{\delta} = \boldsymbol{v}/|\boldsymbol{v}|$, the force valance is described as

$$\boldsymbol{J} \times \boldsymbol{B} - \boldsymbol{\delta} F_{\mathrm{p}} = 0, \tag{1.5}$$

where F_p represents the strength of pinning force. Therefore, we have

$$J = |\boldsymbol{J}| = J_\mathrm{c} \tag{1.6}$$

with $J_\mathrm{c} = F_\mathrm{p}/B$. J_c is the maximum current density under a static state ($\boldsymbol{v} = 0$), in which the electric field is not induced. This is called the critical current density. At the same time, this state is called the critical state.

If the current density is over J_c, the force balance is no longer kept and the flux lines are forced to move. In this case, a force works to prevent the flux lines from moving. This is called the viscous force and its magnitude is proportional to the velocity $\boldsymbol{v}$. It is considered that all flux lines move continuously in the state, and this state is called the flux flow state. Thus, the force balance in the flux flow state is given by

$$\boldsymbol{J} \times \boldsymbol{B} - \boldsymbol{\delta} F_\mathrm{p} - \frac{B}{\phi_0}\eta\boldsymbol{v} = 0, \tag{1.7}$$

where ϕ_0 is the flux quantum ($h/2e = 2.07\times10^{-15}$ Wb, with Planck's constant of $h = 6.63 \times 10^{-34}$ J $\cdot$ s and the elementary electric charge of $e = 1.60 \times 10^{-19}$ C), and η is the viscous coefficient. With the aid of Eq. (1.4) this equation is reduced to

$$J = J_\mathrm{c} + \frac{E}{\rho_\mathrm{f}}, \tag{1.8}$$

where $\rho_\mathrm{f} = B\phi_0/\eta$ is the flow resistivity. This equation, which includes Eq. (1.6) in the static state, describes the E-J characteristics in the superconductor. Thus, the E-J characteristics are theoretically based on the force balance on flux lines.

1.2.2 Flux creep

Even if the current density is not larger than J_c determined by the pining strength, the pinned flux lines are sometimes depinned and move under a finite temperature due to thermal agitation. This is called the flux creep. The thermally activated flux motion is not a macroscopic and continuous motion like a flux flow but a discrete and discontinuous one. When the flux creep takes place, a group of flux lines move collectively. Such a group is called a flux bundle. Figure 1.1 schematically shows a relationship of the

energy of flux bundle versus its position. Usually the flux bundle is trapped at a minimum of the energy. The gradual decrease in the energy shown in the figure when the flux bundle moves to the right is due to the work done by the Lorentz force. Therefore, this slope is proportional to the current density J. If there is no thermal activation, this condition is stable and the flux bundle does not move. However, the flux bundle trapped at the minimum energy is depinned with some probability owing to the thermal activation. An attempt frequency for a flux bundle to try to overcome the barrier within unit time owing to the thermal activation is represented by ν_0. The energy barrier, U, shown in Fig. 1.1 is called the activation energy. The probability for the flux bundle to overcome the energy barrier at one jump is given by the expression of Arrhenius, $\exp(-U/k_{\rm B}T)$, where $k_{\rm B}$ is the Boltzmann constant. The value of activation energy U at zero transport current is the pinning potential U_0. A hopping distance of the flux bundle at one jump seems to be comparable to a flux line spacing $a_{\rm f}$. Therefore, the averaged velocity of flux lines is given by $a_{\rm f}\nu_0\exp(-U/k_{\rm B}T)$. From Eq. (1.4), the induced electric field is given by

$$E = Ba_{\rm f}\nu_0 \left[\exp\left(-\frac{U}{k_{\rm B}T}\right) - \exp\left(-\frac{U'}{k_{\rm B}T}\right)\right], \tag{1.9}$$

where U' is the energy barrier for the flux motion in the opposite direction to the Lorentz force.

One of the issues caused by the flux creep is that the superconducting current cannot be a persistent one but decreases gradually with time. Here, we will argue how the superconducting current changes with time under the flux creep. We treat for simplicity a relaxation of the magnetization of a large superconducting slab ($0 \leq x \leq 2d$) in a magnetic field $H_{\rm e}$ along the z-axis. From the symmetry we have to treat only a half, $0 \leq x \leq d$. In the increasing field process, the current flows to the positive y-axis and the motion of flux lines due to the flux creep occurs to the positive x-axis. If the averaged current density is denoted by J, the magnetic flux density is $B = \mu_0(H_{\rm e} - Jx)$. In terms of its averaged value, $\langle B\rangle$, the electric field at the surface, $x = 0$, is obtained as

$$E = \frac{\partial d\langle B\rangle}{\partial t} = -\frac{\mu_0 d^2}{2}\cdot\frac{\partial J}{\partial t}. \tag{1.10}$$

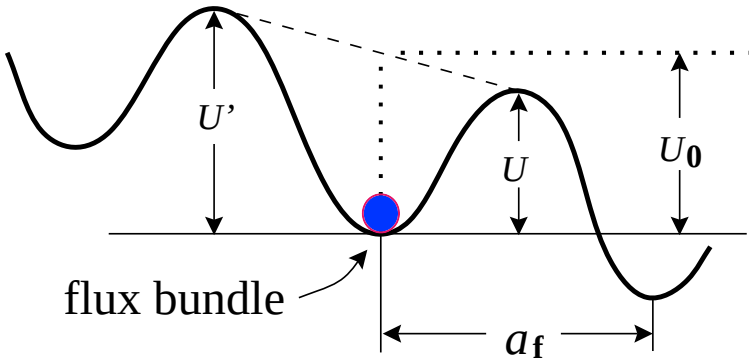

Fig. 1.1. Pinning energy of flux bundle vs its position

The coefficient of the exponential in Eq. (1.9), $Ba_{\rm f}\nu_0$, is considered as a constant with an approximation of $B \simeq \mu_0 H_{\rm e}$. Then, we can solve Eqs. (1.9) and (1.10), if U is given as a function of J.

If it is assumed that there is no thermal activation, flux lines do not flow even in the virtual critical state of $U = 0$. The current density in this state is represented by $J_{\rm c0}$. At a low temperature where the effort of thermal activation is small, it is speculated that the motion of flux lines is not a continuous one like the flux flow even in the vicinity of the virtual critical state. In this case $U \ll U'$ and the second term in Eq. (1.9) can be neglected.

U decreases with increase of the current density J. This variation may be approximated as $U = U_0^* - sJ$ near the virtual critical state. U_0^* represents a value of U extrapolated to the limit $J \to 0$, and is not identical with the real pinning potential U_0, as shown in Fig. 1.2. This is why U_0^* is called the apparent pinning potential. As will be mentioned below, U_0 determines the critical current characteristics under the flux creep, while U_0^* is directly related to the relaxation rate of the magnetization.

From the condition that $U = 0$ at $J = J_{\rm c0}$, we have $s = U_0^*/J_{\rm c0}$ and

$$U(J) = U_0^* \left(1 - \frac{J}{J_{\rm c0}}\right). \tag{1.11}$$

Hence, the equation describing the time variation in the current density is given by

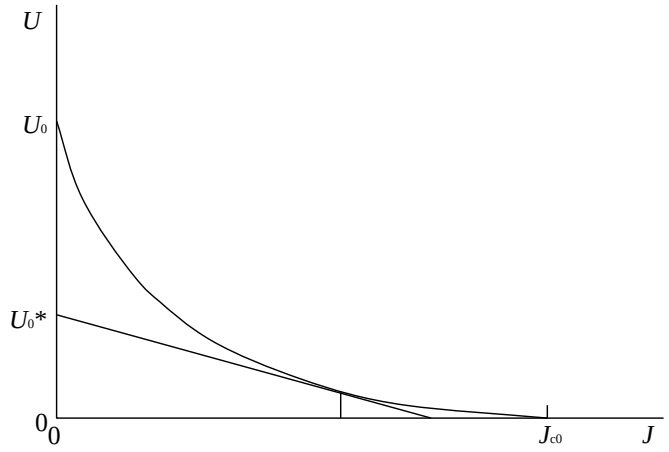

Fig. 1.2. Current density dependence of activation energy. When the depedence is approximated by a tangential line around a given current density, its intercept at $J = 0$ gives the apparent pinning potential, U_0^*.

$$\frac{\partial J}{\partial t} = -\frac{2Ba_{\rm f}\nu_0}{\mu_0 d^2}\exp\left[-\frac{U_0^*}{k_{\rm B}T}\left(1-\frac{J}{J_{\rm c0}}\right)\right]. \tag{1.12}$$

This equation is easily solved, and under the initial condition that $J = J_{\rm c0}$ at $t = 0$, we obtain

$$\frac{J}{J_{\rm c0}} = 1 - \frac{k_{\rm B}T}{U_0^*}\log\left(\frac{t}{\tau}+1\right), \tag{1.13}$$

where τ is a time constant given by $\tau = \mu_0 d^2 J_{\rm c0} k_{\rm B}T/2Ba_{\rm f}\nu_0 U_0^*$. After a sufficient time, $t \gg \tau$, unity in the logarithm in the above equation can be neglected and the time variation in the current density as shown in Fig. 1.3 is derived. The apparent pinning potential energy, U_0^*, can be estimated from the logarithmic relaxation rate:

$$-\frac{\rm d}{{\rm d}\log t}\left(\frac{J}{J_{\rm c0}}\right) = \frac{k_{\rm B}T}{U_0^*} \tag{1.14}$$

U_0^* is usually estimated from a measured magnetic relaxation rate, since the current density J is proportional to the magnetization M. In this case, $J/J_{\rm c0}$ is replaced by M/M_0 with M_0 denoting the initial magnetization.

Here we assume for simplicity that the energy of the flux bundle varies sinusoidally with its x as

$$F(x) = \frac{U_0}{2}\sin kx - f_{\rm L}x, \tag{1.15}$$

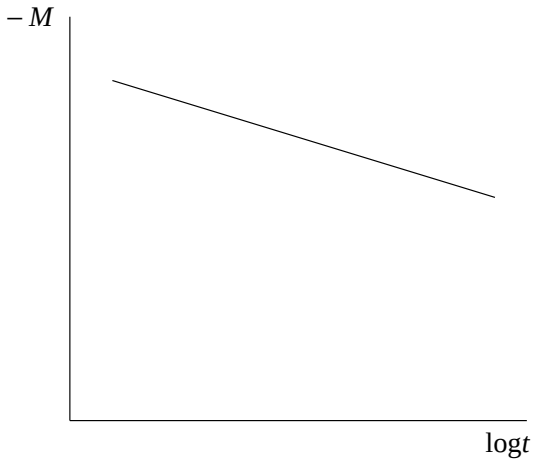

Fig. 1.3. The relaxation of the magnetization due to the flux creep.

as shown in Fig. 1.1. In the above, $k = 2\pi/a_{\rm f}$ is the wave number and $f_{\rm L}$ is the Lorentz force on the flux bundle. If the volume of the flux bundle is V, we have $f_{\rm L} = JBV$. The equilibrium of the flux bundle is obtained by derivating Eq. (1.15) with respect to x and is given by

$$x = -\frac{1}{k}\cos^{-1}\frac{2f_{\rm L}}{U_0 k} \equiv -x_0. \tag{1.16}$$

On the other hand, $F(x)$ is locally maximum at $x = x_0$. Hence, the energy barrier is obtained as $U = F(x_0) - F(-x_0)$. That is,

$$\frac{U}{U_0} = \left[1 - \left(\frac{2f_{\rm L}}{U_0 k}\right)^2\right]^{1/2} - \frac{2f_{\rm L}}{U_0 k}\cos^{-1}\left(\frac{2f_{\rm L}}{U_0 k}\right). \tag{1.17}$$

As mentioned above, the virtual critical state with $U = 0$ will be attained, if there is no thermal activation. In this case $x_0 = 0$ is attained, and hence, $2f_{\rm L}/U_0 k = 1$ is satisfied from Eq. (1.16). The requirement that the J value in this case is $J_{\rm c0}$ leads to

$$\frac{2f_{\rm L}}{U_0 k} = \frac{J}{J_{\rm c0}} \equiv j. \tag{1.18}$$

In terms of the normalized current density, j, Eq. (1.17) is described as

$$\frac{U(j)}{U_0} = (1 - j^2)^{1/2} - j\cos^{-1} j. \tag{1.19}$$

When J is much lower than $J_{\rm c0}$, the flux motion in the opposite direction to the Lorentz force can no longer be neglected. The activation energy in this direction is $U' = U + f_{\rm L} a_{\rm f}$. From $k = 2\pi/a_{\rm f}$ and Eq. (1.18), U' is given by

$$U'(j) = U(j) + jU_0\pi. \tag{1.20}$$

Using this relation, Eq. (1.9) is written as

$$E = Ba_{\rm f}\nu_0 \exp\left[-\frac{U(j)}{k_{\rm B}T}\right]\left[1 - \exp\left(-\frac{\pi U_0 j}{k_{\rm B}T}\right)\right]. \tag{1.21}$$

Therefore, if the pinning potential U_0 and the virtual critical current density $J_{\rm c0}$ are given, the current density vs. the voltage characteristics under the flux creep can be evaluated.

It is theoretically derived[1] that the attempt frequency of the flux bundle is given by

$$\nu_0 = \frac{\zeta\rho_{\rm f}J_{\rm c0}}{2\pi a_{\rm f}B}, \tag{1.22}$$

where ζ is a constant depending on the kind of pinning centers. Namely, $\zeta \simeq 2\pi$ is derived for point-like pinning centers[2] and $\zeta = 4$ is for large and strong pinning centers such as normal precipitates[3]. According to the Bardeen-Stephen model[4], the flux flow resistivity is related to the normal resistivity $\rho_{\rm n}$ as

$$\rho_{\rm f}(T) = \frac{B}{B_{\rm c2}}\rho_{\rm n}(T). \tag{1.23}$$

In high-temperature superconductors $\rho_{\rm n}(T)$ almost linearly changes with temperature. Hence, we assume as $\rho_{\rm n}(T) = (T/T_{\rm c})\rho_{\rm n}(T_{\rm c})$.

If the second term in Eq. (1.20) is sufficiently smaller than $k_{\rm B}T$, the electric field in Eq. (1.21) is written as

$$E \simeq \frac{\pi B a_{\rm f}\nu_0 U_0 J}{J_{\rm c0}k_{\rm B}T}\exp\left(-\frac{U_0}{k_{\rm B}T}\right), \tag{1.24}$$

where the fact that U approaches U_0 in the range of sufficiently small J is taken into consideration. Equation (1.24) shows that the current-voltage characteristic is ohmic, and the electrical resistivity is obtained as

$$\rho = \rho_0 \exp\left(-\frac{U_0}{k_{\rm B}T}\right), \tag{1.25}$$

where $\rho_0 = \pi B a_{\rm f}\nu_0 U_0/J_{\rm c0}k_{\rm B}T$ can be approximately regarded as a constant in a narrow region of temperature. Hence, U_0 can be estimated from the slope of the relationship of $\log\rho$ vs $1/T$. Equation (1.25) shows that the resistivity is not perfectly zero even at very small current density at a finite temperature due to the flux creep.

1.2.3 Critical current density and irreversibility field

As argued in the last section, the superconducting current originated from the flux pinning decreases with time, owing to the flux creep. Since the flux distribution charges with this relaxation and the electric field is generated as shown in Eq. (1.9), the critical current density is smaller than the virtual value J_{c0}. If the critical current density is defined in terms of the electric field criterion, $E = E_c$ (for example, 1.0×10^{-4} V/m), the critical current density J_c can be determined by

$$E_c = Ba_f\nu_0 \exp\left[-\frac{U(J_c)}{k_B T}\right]. \tag{1.26}$$

When the flux creep becomes more drastic, the electric field of the order of the criterion is easily generated even under a small current density, and the critical density is practically zero. The magnetic field B_i at which the critical density is zero is called the irreversibility field. Since the activation energy is equal to the pinning potential when $J = J_c = 0$, the irreversibility field $B_i(T)$ is determined by

$$E_c = Ba_f\nu_0 \exp\left[-\frac{U_0(B_i, T)}{k_B T}\right]. \tag{1.27}$$

It is necessary to describe U_0 as a function of B and T to obtain a theoretical expression of $B_i(T)$.

1.3 Flux creep theory

As described in the last section, the flux creep is an activated motion of flux lines. This causes various phenomena such as a logarithmic relaxation of the magnetization and the irreversibility field. All these phenomena are determined by the pinning potential U_0. Here, we shall theoretically estimate U_0.

According to experimental results, when the flux lines are displaced from the critical state in the opposite direction, the pinning force density changes continuously from $J_c B$ to $-J_c B$ as depicted in Fig. 1.4. That is, the pinning force density varies almost linearly with the displacement u and the phenomenon is reversible, if the displacement is small. The variation rate of the

force density, α_{L}, is called Labusch parameter. This parameter represents the pinning strength. According as the displacement of flux lines increases, some flux lines jump out of individual pinning potentials locally and the pinning force density varies gradually from reversible to irreversible with the displacement. The characteristic displacement d_{i} representing the boundary between reversible and irreversible motion is called the interaction distance. This gives a radius of the averaged pinning potential. When the displacement is further increased, the pinning force density approaches asymptotically $-J_{\mathrm{c}}B$ and the phenomenon becomes describable by the irreversible critical state model. We have the relationship $\alpha_{\mathrm{L}}d_{\mathrm{i}} = J_{\mathrm{c}}B$ (see Fig. 1.4). However, we should note that the pinning potential U_0 cannot be the same as the potential evaluated from experimental results. We assume that a similar phenomenon occurs in the virtual creep-free case where J_{c} is replaced by J_{c0}. Hence, $\alpha_{\mathrm{L}}d_{\mathrm{i}} = J_{\mathrm{c0}}B$ is derived.

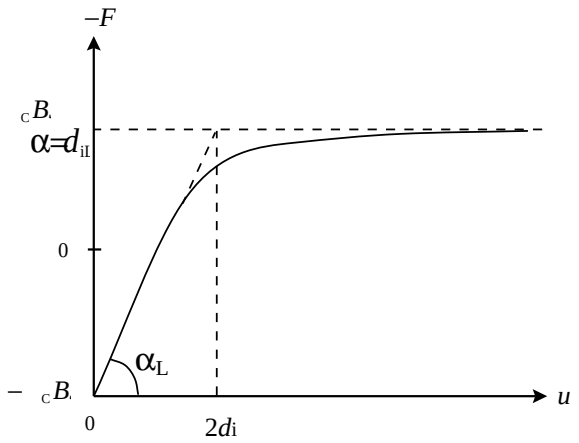

Fig. 1.4. Variation of pinning force density with displacement of flux lines.

Integrating the pinning force density with respect to the displacement u from 0 to d_{i} in Fig. 1.4, the averaged pinning potential per unit volume, $\hat{U_0}$, is estimated as

$$\hat{U_0} = \frac{\alpha_{\mathrm{L}} d_{\mathrm{i}}^2}{2}. \tag{1.28}$$

Using ζ described above, the interaction distance d_{i} is theoretically given by

$$d_{\mathrm{i}} = \frac{a_{\mathrm{f}}}{\zeta}. \tag{1.29}$$

The pinning potential U_0 is given by a product of $\hat{U_0}$ and the volume of the flux bundle V:

$$U_0 = \hat{U_0} V. \tag{1.30}$$

It is to be noted that the volume of the flux bundle V is very important, since it influences the value of the pinning potential.

According to the collective flux creep model the flux bundle in a bulk superconductor is considered as schematically shown in Fig. 1.5(a). The longitudinal and transverse sizes, L and R, which are defined with respect to the direction of applied magnetic field, are different, and the volume of the flux bundle is expressed as

$$V = LR^2. \tag{1.31}$$

The longitudinal flux bundle size is given by

$$L = \left(\frac{C_{44}}{\alpha_{\mathrm{L}}} \right)^{1/2} = \left(\frac{B a_{\mathrm{f}}}{\zeta \mu_0 J_{\mathrm{c0}}} \right)^{1/2}, \tag{1.32}$$

where is C_{44} is the elastic modulus of flux lines for bending deformation, given by

$$C_{44} = \frac{B^2}{\mu_0}. \tag{1.33}$$

On the other hand, the transverse flux bundle size, R, is given by

$$R = \left(\frac{C_{66}}{\alpha_{\mathrm{L}}} \right)^{1/2}, \tag{1.34}$$

where C_{66} is the shear modulus of the flux line lattice. Its value depends sensitively on the state of the flux line lattice. When the flux lines form a perfect triangular lattice, we have

$$C_{66}^0 = \frac{B_{\mathrm{c}}^2 B}{4\mu_0 B_{\mathrm{c2}}} \left(1 - \frac{B}{B_{\mathrm{c2}}} \right)^2. \tag{1.35}$$

C_{66} becomes smaller according as the lattice becomes imperfect, and it is zero when the lattice melts.

The state of the flux line lattice, which is strongly influenced by the flux creep, cannot be determined apriori. This means that C_{66} cannot be estimated deterministically. Usually R takes on a value of the order of the flux line spacing a_{f}, and it is expressed as

$$R = g a_{\mathrm{f}}, \tag{1.36}$$

where g^2 represents the number of flux lines inside the flux bundle. When the state of the flux line lattice is close to a melt state and/or when pins are very strong, the theoretically estimated value of R is lower than a_{f}. But, the minimum g^2 should be one. From Eqs. (1.34) and (1.36), g^2 is given by

$$g^2 = \frac{C_{66}}{\zeta J_{\mathrm{c0}} B a_{\mathrm{f}}}. \tag{1.37}$$

When the flux lines form a perfect triangular lattice, Eq. (1.37) leads to

$$g_{\mathrm{e}}^2 = \frac{C_{66}^0}{\zeta J_{\mathrm{c0}} B a_{\mathrm{f}}}, \tag{1.38}$$

which gives the maximum value of g^2.

As mentioned above, the value of C_{66} cannot be estimated deterministically. From the thermodynamic viewpoint, it is assumed that g^2 is determined so that the critical density under the flux creep takes on a the maximum value [5]. The second term in Eq. (1.9) is neglected for simplicity. If Eq. (1.11) is used, the critical current density under the flux creep is given by

$$J_{\mathrm{c}} = J_{\mathrm{c0}} \left[1 - \frac{k_{\mathrm{B}} T}{U_0^*} \ln \left(\frac{B a_{\mathrm{f}} \nu_0}{E_{\mathrm{c}}} \right) \right]. \tag{1.39}$$

We have $J = J_{\mathrm{c}} = 0$ and the apparent pinning potential U_0^* is equal to the real pinning potential U_0 at the irreversibility field. It is assumed that the value of g is $y(< 1)$ times as large as the value of g_{e} given by Eq. (1.38):

$$g = y g_{\mathrm{e}}. \tag{1.40}$$

In the above the longitudinal flux bundle size is considered as a constant, since the elastic modulus of flux lines for bending deformation, C_{44}, depends only on the magnetic energy and does not depend on defects of the flux lattice. Therefore, the correlation volume is proportional to y^2 from Eqs. (1.36) and (1.31). The virtual critical current density in the flux creep-free case, J_{c0}, is y^{-1} time as large as the value, J_{ce}, when $g = g_{\mathrm{e}}$. As will be mentioned, the pinning potential U_0 is given by Eq. (1.46). Hence, U_0 is $y^{3/2}$ times as large as the value U_{e} when $g = g_{\mathrm{e}}$. Therefore, the critical current density is given by

$$J_{\rm c} = \frac{J_{\rm ce}}{y}\left[1 - \frac{k_{\rm B}T}{U_{\rm e}y^{3/2}}\ln\left(\frac{Ba_{\rm f}\nu_0}{E_{\rm c}}\right)\right]. \tag{1.41}$$

From the condition that this derivative with respect to y is zero, the maximum condition for $J_{\rm c}$ is given by

$$y = \left[\frac{5k_{\rm B}T}{2U_{\rm e}}\ln\left(\frac{Ba_{\rm f}\nu_0}{E_{\rm c}}\right)\right]^{2/3}. \tag{1.42}$$

Therefore, from Eq. (1.40), g^2 is given by

$$g^2 = g_{\rm e}^2\left[\frac{5k_{\rm B}T}{2U_{\rm e}}\ln\left(\frac{Ba_{\rm f}\nu_0}{E_{\rm c}}\right)\right]^{4/3}. \tag{1.43}$$

Thus, we have

$$U_0 = \frac{0.835g^2k_{\rm B}J_{\rm c0}^{1/2}}{\zeta^{3/2}B^{1/4}}. \tag{1.44}$$

When the thickness of the superconductor d is smaller than the longitudinal bundle size L as shown in Fig. 1.5(b), the volume of the bundle is given by

$$V = dR^2. \tag{1.45}$$

Thus, the pinning potential is obtained as

$$U_0 = \frac{4.23g^2k_{\rm B}J_{\rm c0}d}{\zeta B^{1/2}}. \tag{1.46}$$

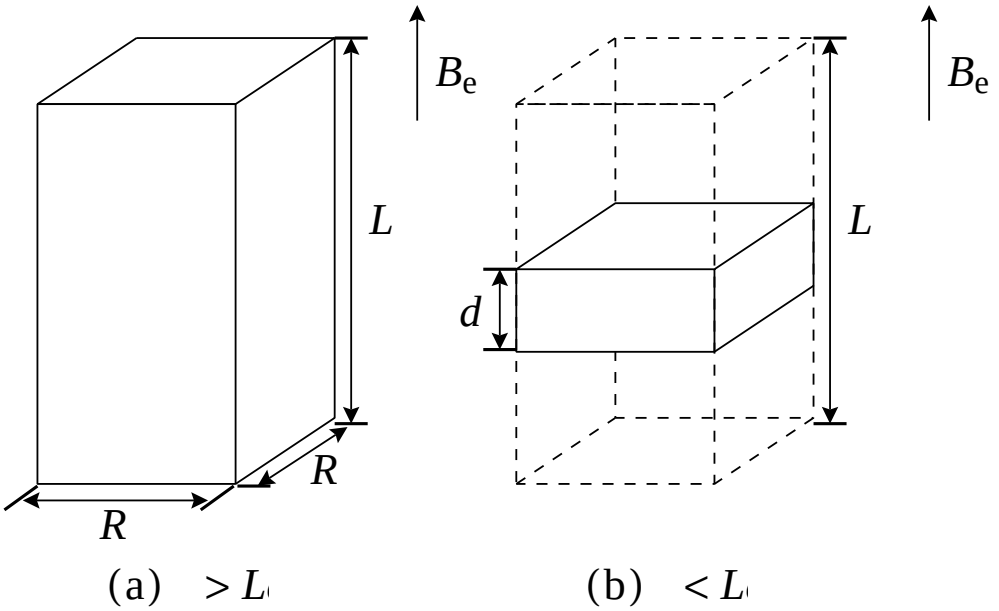

Fig. 1.5. Diagram of the flux bundle when the longitudinal flux bundle size L is (a) smaller and (b) larger than the thickness d of the superconductor.

According to the scaling relation of the pinning force density known for metallic superconductors, we assume that the temperature and magnetic field dependencies of the creep-free critical current density are expressed as

$$J_{c0} = A\left[1-\left(\frac{T}{T_c}\right)^2\right]^m B^{\gamma-1}\left(1-\frac{B}{B_{c2}}\right)^\delta, \tag{1.47}$$

where the empirical temperature dependence of the upper critical field is given by

$$B_{c2}(T) = B_{c2}(0)\left[1-\left(\frac{T}{T_c}\right)^2\right]. \tag{1.48}$$

In the above m, γ and δ are numerical parameters depending on the kind and strength of pinning centers.

Using the pinning potential U_0 for d larger than L, we will analytically estimate the irreversibility field B_i. For simplicity, if the distribution of the pinnig force is disregarded, using Eqs. (1.47), (1.27) and (1.44), we have

$$B_i^{(3-2\gamma)/2} = \left(\frac{K}{T}\right)^2\left[1-\left(\frac{T}{T_c}\right)^2\right]^m, \tag{1.49}$$

where K is an approximately constant value given by

$$K = \frac{0.835 g^2 A^{1/2}}{\zeta \ln(B_{\rm i} a_{\rm f} \nu_0 / E_{\rm c})}, \tag{1.50}$$

where the value of $\ln(B_{\rm i} a_{\rm f} \nu_0 / E_{\rm c})$ is approximately a constant because of the logarithmic function. It is to be noted that Eq. (1.49) is valid when $B_{\rm i}$ is sufficiently smaller than $B_{\rm c2}$.

1.4 Various measurements of the E-J characteristic

Recently various measurements were performed to evaluate the E-J characteristic of high temperature superconductors in a wide range of the electric field. Here, some measuring methods are briefly introduced.

1.4.1 Measurement of the E-J characteristic in the range of high electric field

1. Four probe method (resistive method)

   In this method, the current is transported directly to the specimen in a magnetic field, and then E and J are simply calcuated from the generated voltage and the applied current, respectively. Althouth the measurement is simple, the measurement in the range of low electric field is difficult because of a limited sensitivity of instruments. Usual measurements are done in the range of $10^{-5} \sim 10^{-2}$ V/m (see Fig. 1.7).

1.4.2 Measurement of the E-J characteristic in the range of low electric field

As for the measurements in the range of low electric field, there are following methods, in all of which the E-J characteristics are estimated indirectly by analyzing measured results of the magnetization of the specimen. In one method a relaxation of the magnetization is measured in a constant magnetic field, and in the other methods the magnetization is measured in a sweeping magnetic field.

1. Relaxation measurement in a constant magnetic field

   In this method, the current density is estimated from the measured magnetization, and the electric field is estimated from the time variation of the magnetization and then, the E-J characteristic is given. The magnetization can be measured using a SQUID(Superconducting Quantum Interference Device) magnetometer, a Hall sensor and a VSM (Vibrating Sample Magnetometer). The SQUID (see Fig. 1.6) is useful to measure the characteristic in lower range of the electric field than the Hall sensor (see Fig. 1.7).

2. Magnetization measurement in a sweeping magnetic field

   In this method, it is possible to change largely the level of electric field by changing the sweep rate of external magnetic field. The current density is estimated from the measured magnetization. The magnetization can be measured using the VSM, the Hall sensor and pick up coils. For example, Fig. 1.8 shows the E-J characteristics measured by Mawatari *et al.* [6] using the VSM.

1.4.3 E-J characteristics in a wide range of the electric field

Using the four probe method and the magnetization method with a Hall sensor, Nakamura *et al.*[7] evaluated systematically the temperature dependence of the E-J characteristics in a wide range of the electric field, as shown in Fig. 1.7. As can be seen at 61.2 K for example, concave $\ln E$-$\ln J$ curves are observed in the low range of the electric field by the magnetization method, although flux lines are expected to be in the so-called glass state judging from the curves in the high electric field range obtained by the four probe method. Namely, S-shaped $\ln E$-$\ln J$ curves are observed. This suggests that the transition temperature, T_{g}, depends on the range of the electric field. On the other hand, in the vortex glass-liquid transition model, it is predicted that the critical indexes given by the scaling are general material parameters, as will be described in the next section 1.5. However, the above result suggests that the critical indexes depend also on the electric field.

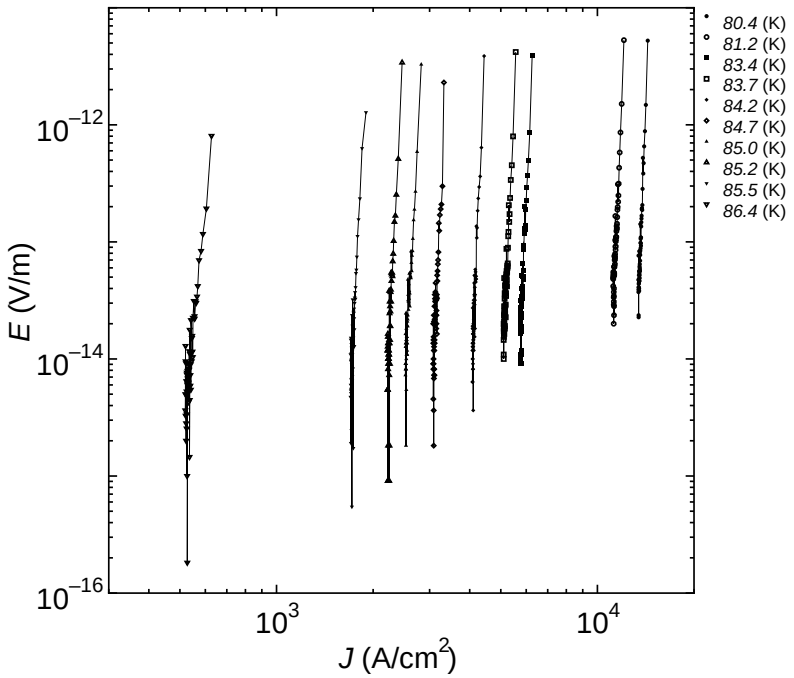

Fig. 1.6. The E-J characteristics by the magnetization method using a SQUID magnetometer[8].

Fig. 1.7. Temperature dependent E-J characteristics in YBaCuO thin film at 0.52 T obtained by the four probe method (top) and the magnetization method (bottom). Temperature was changed in the range of 61.2 K $\sim$ 90.4 K for the four probe method, and 25.5 K $\sim$ 72.3 K for the magnetization method[7].

Fig. 1.8. The E-J characteristics by Mawatari *et al.*[6)]

1.5 Vortex glass-liquid transition model

The vortex glass-liquid transition model assumes that the thermodynamic phase transition of the flux line system occurs and a scaling of the E-J curves near the transition point is considered as a proof of the transition. However, the transition point itself is not discussed in the theory. Various experimental results show that the transition point is determined by the pinning strength. This is essentially the same as the prediction of the flux creep model. But, there are some different points between the flux creep model and the vortex glass-liquid transition model. One of them is that the electric resistivity becomes zero in the vortex glass-liquid transition model when the current density J approaches zero, while a finite value of electrical resistivity remains in the flux creep model as shown in Eq. (1.25).

Fisher *et al.*[9] assumed that the glass phase of flux lines could be characterized by the coherence length. It is also assumed that the coherence length diverges as $\xi_{\rm g} \sim |T - T_{\rm g}|^{-\nu}$ in the vicinity of the transition temperature $T_{\rm g}$, where ν is a static critical index. At the same time the relaxation time of flux line system is assumed to diverge as $\tau \sim {\xi_{\rm g}}^z$, where, z is a dynamic critical index. According to Fisher *et al.*, the E-J characteristic is given by

$$E(J) \simeq J{\xi_{\rm g}}^{d-2-z} f_{\pm}(\frac{J}{J_0}), \tag{1.51}$$

where d is the dimensionality of flux lines, and f_+ and f_- are functions defined in ranges of $T > T_{\rm g}$ and $T < T_{\rm g}$, respectively. In the above J_0 is the current density corresponding to the critical current density in the vortex glass state when $T < T_{\rm g}$, and is given by

$$J_0 = \frac{k_{\rm B}T}{\phi_0 \xi^{d-1}}, \tag{1.52}$$

where ϕ_0 is a flux quantum. J_0 is zero when $T \to T_{\rm g}$. On the other hand, since the resistivity is ohmic in the vortex liquid state even when $J \to 0$, f_+ is needed to approach a constant as $J \to 0$. In this case, therefore, the ohmic resistivity is given by $\rho \sim (T - T_{\rm g})^{\nu(z+2-d)}$.

Fisher *et al.* assumed also that the current-voltage characteristics are given by

$$E \sim \exp\left[-\left(\frac{J_{\mathrm{T}}}{J}\right)^{\mu}\right], \tag{1.53}$$

where J_{T} is a parameter which has a dimension of current density depending on temperature and μ is a parameter satisfying $\mu \leq 1$. That is, the resistivity ρ disappears in the glass state in which the flux lines freeze.

On the other hand, since $J/J_0 \equiv x$ approaches infinity in the transition point at finite E and J, and Eq. (1.51) is given by $E \propto x^{(d-2-z)/(d-1)} f_{\pm}(x)$, $f_{\pm}(x) \sim x^{(z+2-d)/(d-1)}$ is led in this limit. Therefore, when $T = T_{\mathrm{g}}$, the current-voltage characteristics are given by a power law function:

$$E \propto J^{(z+2-d)/(d-1)}. \tag{1.54}$$

These indexes are estimated by experiments of the E-J characteristics as shown in Fig. 1.9. This figure shows the experimental example of the E-J characteristics in an Y-123 film at various temperatures and magnetic field of 4 T. From the measured results, it is known that the E-J curves change from convex to concave across the transition point with increasing temperature. First, z is estimated at the transition temperature at which the E-J characteristic is given by the power law function as Eq. (1.54). Next, the value of ν is adjusted, so that $(E/J)/|T - T_{\mathrm{g}}|^{\nu(z-1)}$ vs $J/|T - T_{\mathrm{g}}|^{2\nu}$ curves would scale. Figure 1.10 is the scaled result of the experiment in Fig. 1.9. In this case, the evaluated indexes are $\nu = 1.7$ and $z = 4.8$.

On the other hand, it is reported that the current-voltage characteristics estimated by the flux creep-flow model is also well scaled as mentioned above, and the scaling parameters evaluated from the experiment are theoretically explained. However, these two theoretical models are not exactly the same. From the viewpoint of the vortex glass-liquid transition model, it is considered that the vortex glass state is determined only by their own nature, and when flux lines are in this state, those can be pinned and irreversible magnetic phenomena occur. When those are in the liquid state, those cannot be pinned, resulting in reversible phenomena. On the contrary, in the flux creep model, it is suggested that, since the flux pinning works effectively against the thermal agitation in the region below the transition curve, flux lines can be regarded to be in the glass state. When the flux pinning is not effective as in the

Fig. 1.9. Example of observed E-J characteristics in an Y-123 film at various temperatures and magnetic field of 4 T[10)].

Fig. 1.10. Scaled result of E-J characteristics using the analysis of the vortex glass-liquid transition model[11)].

region above the transition curve, those are regarded to be in the liquid state. That is, the concept of the flux pinning is considered to be more essential. Note that the thermal depinning itself is a second-order phase transition[12], and this gives a theoretical proof for the scaling of the E-J curves. On the other hand, in the vortex glass-liquid model, it is considered that the scaling parameters take on constant values peculiar to materials independently of temperature, magnetic field and electric field. However, in fact, the scaling parameters depend on the electric field as mentioned in section 1.4.3. It was also reported that these parameters depend also on temperature [13]. In addition, the transition point depends on the flux pinning strength [14]. These results show that the critical indexes given by the scaling are not general material parameters, but are strongly related to pinning mechanism.

1.6 Summation problem

The macroscopic pinning force density, $F_{\rm p} = J_{\rm c}B$, which is the force on flux lines by pinning centers in a unit volume is a function of the elementary pinning force, $f_{\rm p}$, the number density of pinning centers, $N_{\rm p}$, and the density of flux lines, i.e., the magnetic field, B. It depends also on temperature, T, through the elementary pinning force. The problem to theoretically estimate $F_{\rm p}$ as a function of these factors is called a summation problem. It is to be noted that the critical current density which is directly estimated from $F_{\rm p}$ is the virtual value in the absence of flux creep.

1.6.1 Metallic superconductors

In metallic superconductors, the distribution width of the local pinning force density is narrow enough. In addition, the ambient temperature is very low due to low critical temperatures. Hence, the effect of thermal activation can be disregarded in most cases. In such a case, the distribution of the critical current density and the E-J characteristic are represented in Fig. 1.11(a) and (b), respectively. When the applied current density is larger than the critical current density ($J_{\rm c0}$), all flux lines are depinned and go to the flux flow state with a generated resistivity. In addition, artificial pinning centers

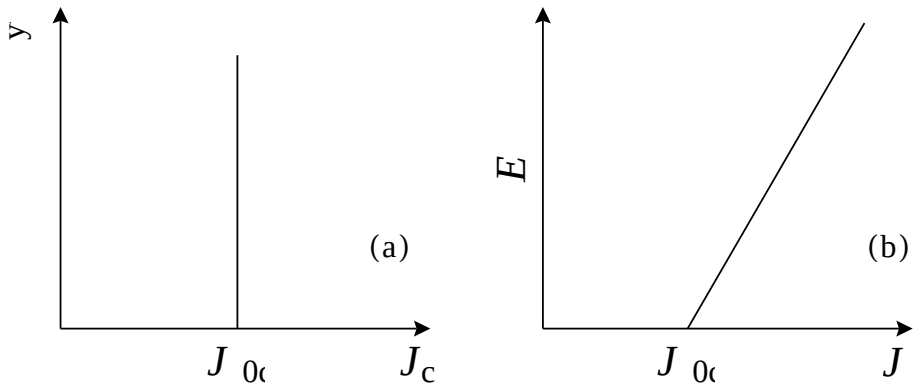

Fig. 1.11. (a) Distribution of critical density and (b) E-J characteristic in metallic superconductors.

can be successfully introduced into materials.

1.6.2 High-temperature oxide superconductors

On the other hand, the high-temperature superconductor depends largely on the thermal activation motion, a weak rink, the layer crystal structure and so on. Moreover, the wide distribution of the force is considered in the elementary pin, since the technology to introduce a pin with uniform strength intentionally is not established. In practical cases, the E-J characteristic appear gradually due to above causes as shown in Fig. 1.12 and is different from the metallic superconductor such as Fig. 1.11, and this behavior is complicated. It is not merely assumed that the critical current density is a constant J_c parameter as before. That is, the wide distribution of J_c is expected.

1.7 Percolation flow model

As mentioned in above section, in the usual metallic superconductor, since it is possible to introduce the uniform pin of the strength, the estimation of the material and the E-J characteristic is estimated using the constant parameter representing the critical current density, J_c. However, in the high-temperature superconductor, the behavior is complicated, and the E-J char-

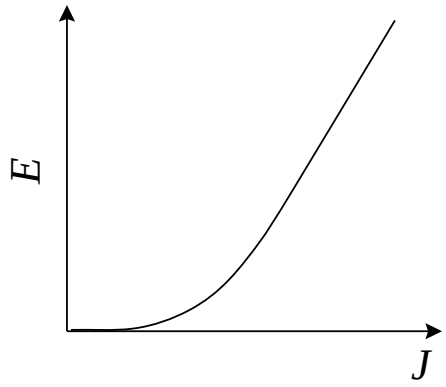

Fig. 1.12. The diagram of the E-J characteristic in the high-temperature oxide superconductor.

acteristic cannot be described using a parameter for critical current density J_c, due to the thermal activation motion, a weak rink, the layer crystal structure and so on. Therefore, it is assumed that the distribution of the critical current density is shown in Fig. 1.13 in the high-temperature superconductor. Moreover, it is assumed that the current transport characteristic is governed by the percolation process, which the pinned flux lines are depinned out of the pin and then the unpinned cluster grows gradually. From these assumption, it is proposed that the E-J characteristic is described using a percolation flow model. Here, it is mentioned simplely about this model.

ctitical

As the current is increased, the unpinned cluster grows. When the unpinned cluster size reaches the percolation limit, the electric field due to the flux flow is induced along the percolation path. The threshold value of induced current in this case represents the minimum of the critical current. This process is shown in Fig. 1.14.

In ideal system with the uniform pinning force for an usual metallic superconductor, all of pinned flux lines are depinned at a blast at a critical value. In other words, a function of the depinning probability is given by a step function. On the contrary, in the confused system like the high-temperature superconductor, pinned flux lines are depinned with a spread from the percolation threshold. That is, a distribution of the critical current occurs.

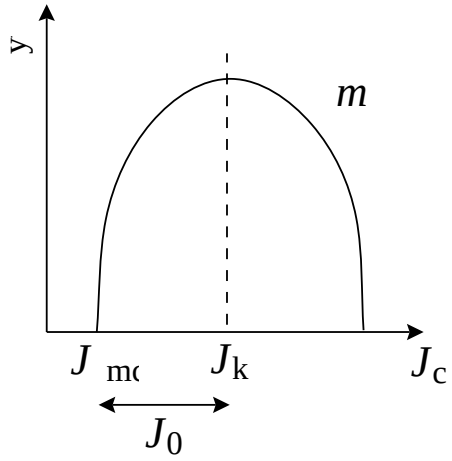

Fig. 1.13. The distribution of the critical current density assumed in the percolation flow model.

Fig. 1.14. Unpinned cluster

Therefore, in this model, the distribution of the critical current density is assumed using three parameters as shown in Fig. 1.13. In this case, $J_{\rm cm}$ represents the minimum of $J_{\rm c}$ (the percolation threshold), and J_0 represents the half width of the distribution, and m' is the parameter depending on the form of the distribution. If it is assumed that the flow resistivity, $\rho_{\rm f}$, is a constant in the elementary E-J characteristic, from the distribution of the critical current density, the theoretical equation of E-J characteristic is estimated. In this case, it is reported that the probability density function $Q(J)$ can be described by the Weibull function. In the vicinity of the percolation threshold, $Q(J)$ can be approximated by $((J - J_{\rm cm})/J_0)^{m'}$. Therefore, the E-J characteristics can be written in analytical form as follows.

$$\begin{aligned} E(J) &= \rho_{\rm f} \int_0^J Q(J){\rm d}J \\ &= \frac{\rho_{\rm f}}{m'+1} J \left(\frac{J}{J_0}\right)^{m'} \left(1 - \frac{J_{\rm cm}}{J}\right)^{m'+1}; && B < B_{\rm GL} \\ &= \frac{\rho_{\rm f}}{m'+1} J \left(\frac{J}{J_0}\right)^{m'}; && B = B_{\rm GL} \\ &= \frac{\rho_{\rm f}}{m'+1} |J_{\rm cm}| \left(\frac{|J_{\rm cm}|}{J_0}\right)^{m'} \left\{ \left(1 + \frac{J}{|J_{\rm cm}|}\right)^{m'+1} - 1 \right\}; && B > B_{\rm GL} \end{aligned} \tag{1.55}$$

where $B_{\rm GL}$ represents the magnetic field when $J_{\rm cm} = 0$. Using this percolation flow model, the E-J characteristics can easily be calculated in a high range of the electric field ($10^{-5} \sim 10^{-2}$ V/m) using a usual resistive method. This is an advantageous point of the percolation model in comparison with the flux creep-flow model in which a complicated calculation is needed.

However, in this model, the flux motion under a significant thermal activation as shown in Fig. 1.1, is approximated by an equivalent flux flow by making the pinning potentials shallow as shown in Fig. 1.15. Therefore, in the creep region of a very low electric field such as 10^{-10} V/m, the theoretical prediction deviates from experiment due to a part of flux creep which was neglected. Hence, the extensive percolation flow model was proposed [15] Since the pinning potential is shallowed by U_1 for activated flux lines, the height of potential barrier which these flux lines feel is ΔU as illustrated in

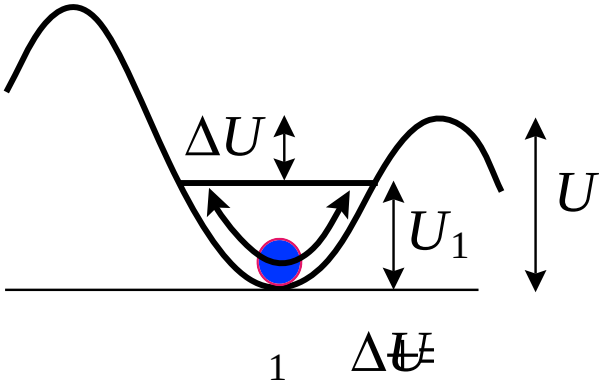

Fig. 1.15. Pinning potential is regarded to be made shallow by U_1 due to the movement of pinned flux bundle in the percolation model.

Fig. 1.1(b). Arrhenius' expression was assumed for the probability for flux lines to overcome the barrier. The electric field due to the flux creep is added to that due to the equivalent flux flow. It is simply assumed that a magnitude of ΔU is proportional to that of J_c. The applicability of this assumption will be argued elsewhere. In addition, the attempt frequency ν_0 is assumed as a fitting parameter and a value of the order of 10^7 Hz is used to explain experimental results at low electric fields [15].

On the other hand, in this study, the obtained results are explained by a theoretical analysis based on the flux creep-flow model in which the distribution of flux pinning strength is taken into account. In this model, as the detail mentioned in section 3.1, the E-J characteristics are determined by the flux creep, a discontinuous flux motion by thermal agitation and the flux flow, a continuous flux motion, by the Lorentz force. Therefore, the percolation flow model and the flux creep-flow model are essentially based on the same mechanism. Comparison between two models is mentioned in section 3.2.

1.8 Aim of the study

In this study, using a four probe method (resistive method) and the relaxation method of the magnetization using a SQUID magnetometer, the E-J characteristics in superconducting multifilamentary Bi-2223 silver-sheathed tape are evaluated. Using the both methods, it is possible to evaluate the E-J characteristics in a wide range of the electric field. The evaluated results is compared with the theoretical results by the flux creep-flow model, which is taken the distribution of the flux pinning into account.

On the other hand, from an analysis of E-J curves with the aid of the flux creep-flow model, the ratio of contribution from the flux flow to the total electric field is estimated. It is clarified that most of the electric field is caused by the flux creep even in the range of electric field in usual resistive measurement. It was found that a difference of the attempt frequency of flux bundle between the two models can be explained by a depth of shallowed pinning potential. Moreover, it is clarified that the percolation flow model is consistent with the flux creep-flow model from the comparison between the two models. This gives a theoretical proof for the parameters of the percolation flow model.

A pinning potential U_0 is an important parameter determined an irreversibility field, a relaxation rate of a superconducting current and so on, including the above E-J characteristics. But, the quantitative U_0 was not estimated widely, although the apparent pinning potential U_0^* is estimated from a relaxation of the magnetization and so on. In the past, the U_0 was estimated from an analysis of the E-J characteristics and the irreversibility field $B_{\rm i}$. In this study, using the magnetization relaxation method, an ohmic E-J characteristics in a TAFF(thermally activated flux flow) region are measured. Comparing between the evaluated results and the creep theory, the quantitative U_0 is estimated and is compared with the values estimated by the past methods.

Chapter 2

Experiment

2.1 Specimen

Specimen was a superconducting multifilamentary Bi-2223 silver sheathed tape prepared by the powder-in-tube (PIT) method, and was manufactured by Vacuumschmelze company. Since such a long tape with a good quality can be manufactured, the material is now widely used for applications such as a magnet, a cable and so on.

The silver sheath of the tape works as a protective material to absorb a stress on the tape. It also works as a shunt material when an excess current is applied to the tape. However, this makes the experiment difficult to estimate the E-J characteristic only of the superconducting filaments. For this purpose, a simple model was used in which the tape was approximated by a parallel circuit of the superconductor and the silver matrix.

The number of superconducting filaments f in the tape specimen was 59, and the averaged width w and thickness d were 320 μm and 11 μm, respectively. The critical temperature measured by a DC magnetization method, $T_{\rm c}$, was 110 K.

2.2 Experimental method

In this study, the four probe method (the resistive method) and the DC magnetization method using a SQUID magnetometer were used, in order to evaluate the E–J characteristics in the Bi-2223 silver sheathed tape. The former is used in the range of high electric field ($10^{-5} \sim 10^{-2}$ V/m), while

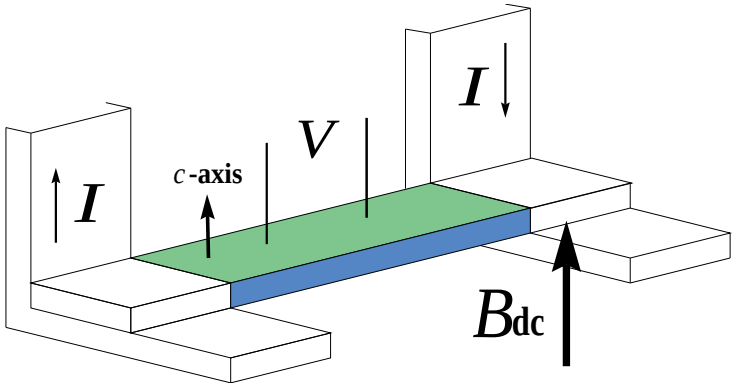

Fig. 2.1. Four probe method (resistive method)

the latter is used in the range of very low electric field ($10^{-11} \sim 10^{-9}$ V/m).

2.2.1 Four probe method (resistive method)

Terminals of current and voltage were attached to the specimen as seen in Fig. 2.1. At a constant temperature T and a magnetic field B parallel to the c-axis, a pulsed current I by one second was applied to the specimen, and the generated voltage V was measured by the voltage terminals of distance L about 10 mm. The E–J characteristic was estimated using the following equations:

$$J = \frac{I}{wdf}, \tag{2.1}$$

$$E = \frac{V}{L}. \tag{2.2}$$

The pulsed current was useful in order to prevent the temperature of the specimen from increasing by the Joule heat when the current was applied. On the other hand, during the soldering between the specimen and the voltage terminal, we enlarged the contact area so that the current could flow uniformly. In the measurement, the specimen was placed in an atmosphere of helium gas, and the temperature was controlled using a heater and by controlling a flow rate of helium gas. The temperature of the specimen was measured using a thermocouple fixed to the surface of specimen.

2.2.2 Magnetization method using a SQUID magnetometer

In this measurement, a SQUID(Superconducting Quantum Interference Device) magnetometer (MPMS-7) was used. The tape was cut in the length l of 4.2 mm. A DC magnetic field of a sufficient strength was applied parallel to the c-axis of the specimen and was decreased to a desired strength. This put the specimen in the critical state with fully trapped magnetic flux. In this condition the induced superconducting current flowed inside the specimen. Then, the relaxation of the magnetization was measured. In section 2.2.3, the strength of the initially applied magnetic field necessary for the measurement will be described. The shielding current density was estimated from an irreversible component of the magnetic moment m. The electric field at edge of the filament was estimated from a variation of m with time using the Maxwell equation. Thus, the E–J curves were estimated from the relaxation measurement of the magnetization. The detailed analysis is described in Appendix A. The equations used for the estimation are:

$$J = \frac{12m}{w^2 df(3l - w)}, \tag{2.3}$$

$$E = -\frac{\mu_0}{2df(l + w)} \cdot \frac{\mathrm{d}m}{\mathrm{d}t}. \tag{2.4}$$

In the above the flux distribution in all superconducting filaments was assumed to be in the critical state described by the Bean model.

SQUID magnetometer

The SQUID is made up of a superconducting loop with the Josephson junction. Using this, the periodical value of the current density with the increase of the flux can be measured. Therefore, the SQUID is a the high-performance magnetic sensor. In this MPMS, an superconducting magnet was shared inside the instrument, and a magnetic moment was measured by automatic controlling. In this system, the sample is positioned below the detection coils and is set at its lower limit of travel. Then, the sample is raised through the coils while measuring the output of the SQUID detector.

In its initial position, the sample should be far enough below the detection coils so that the SQUID did not detect the sample moment. The sample

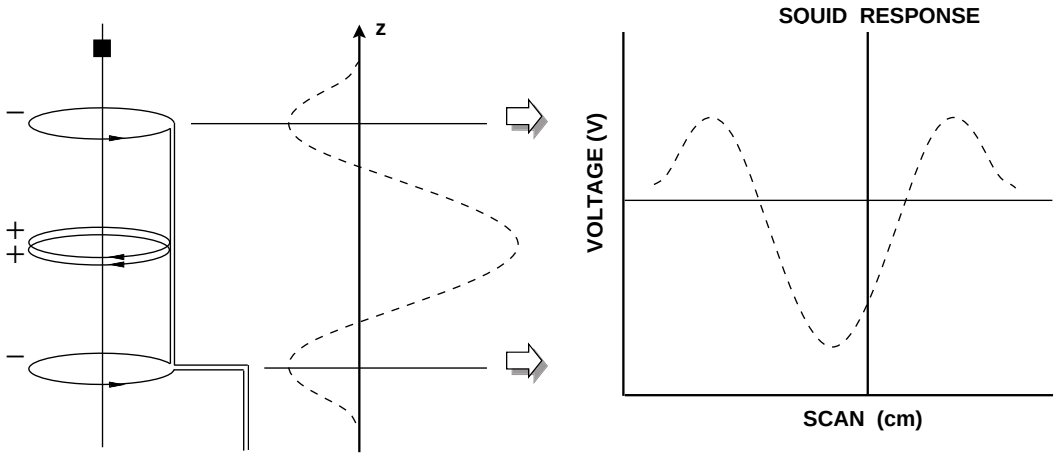

Fig. 2.2. A second-order gradiometer coil and SQUID output response to sample scan.

was then typically measured by repeatedly moving the sample upward some distance and reading the voltage from the SQUID detector. If the SQUID voltage was read at a large number of points, the voltage could be plotted as a function of the sample position, as shown in Fig. 2.2. A set of such data was a scan. The shape of the curve was a function of the detection coil geometry used by this system. As shown the left hand in Fig. 2.2, the coils were wound in a second-derivative configuration in which the upper and lower single turns were counterwound with respect to the two-turn center coil. The coils were called a second-order gradiometer coil. This configuration strongly rejected interference from nearby magnetic sources and lets the system function without the need for a superconducting shield around the SQUID sensing loop.

Using the Full Length DC Scan method, the magnetic moment was computed as the square root of the sum of the squares for the number of data points. This process minimizes errors due to volume variations in the sample.

2.2.3 Sufficient value of the initial magnetic field applied to the specimen

Before starting the relaxation measurement, an external magnetic field of a sufficient magnitude B_{m} was first applied to the specimen, and then, decreased to a desired value for the measurement, B_{e}, as described in section

2.1.2.

The flux distribution in the specimen can be analyzed using the Bean model. The left figures in (a) $\sim$ (d) of Fig. 2.3 show the flux distribution while the magnetic field is increased to B_{m}, and the right figures show the flux distribution while the magnetic field is decreased to B_{e}.

From this result it is seen that the initial magnetic field B_{m} should be stronger than $B_{\mathrm{e}} + 2B_{\mathrm{p}}$ so that the specimen is the critical state.

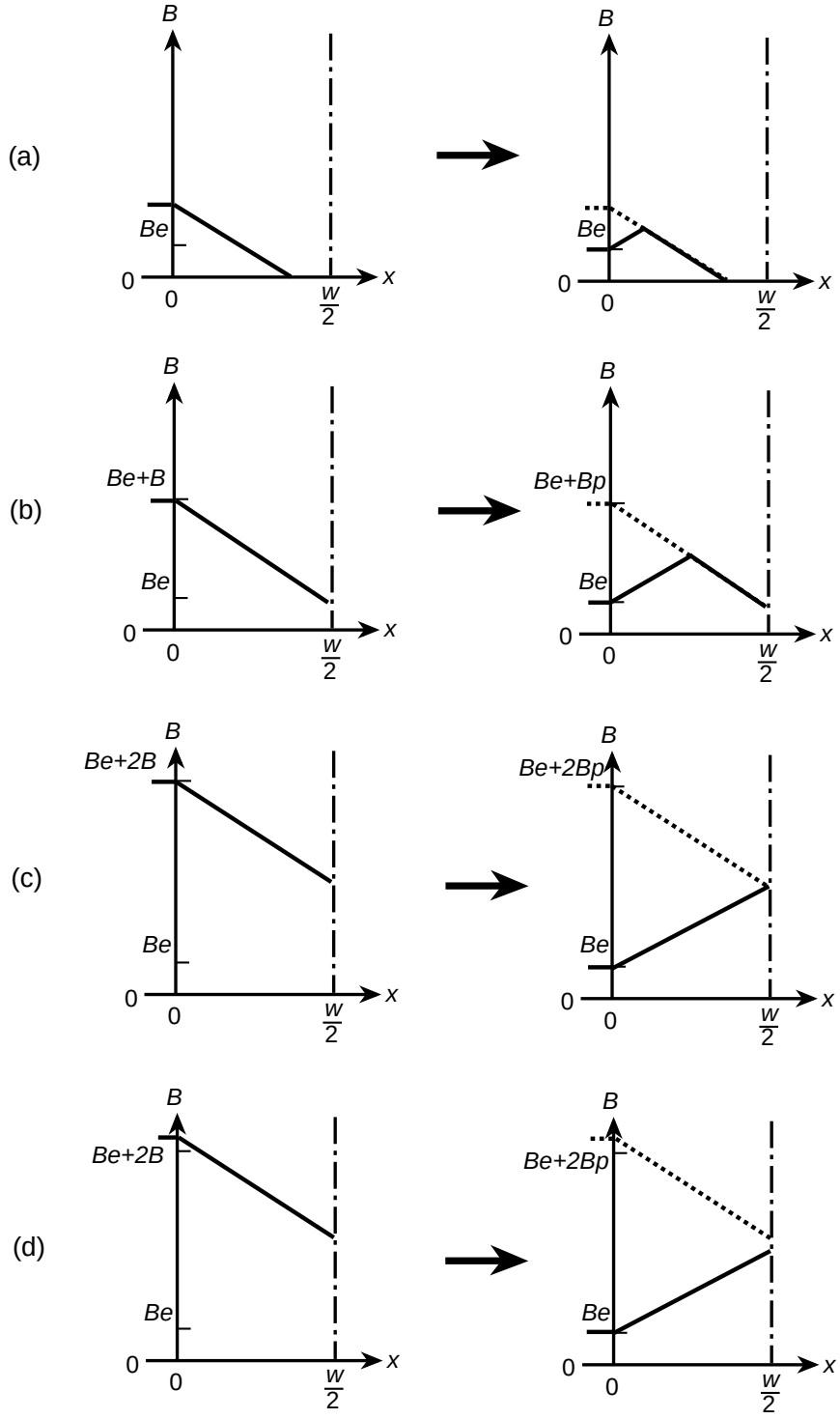

Fig. 2.3. Variation of flux distribution in a half of the specimen. The left figures in (a) $\sim$ (d) show the flux distribution while the magnetic field is increased to B_{m}, and the right figures show the flux distribution while the magnetic field is decreased to B_{e}.

Chapter 3

Result and discussion

In this chapter, the E-J characteristics in superconducting multifilamentary Bi-2223 silver-sheathed tape are evaluated in a wide range of the electric field from the experimental results of the four probe method and the magnetization relaxation method. The evaluated results are compared with the theoretical results of the flux creep-flow model[17]. In the theoretical analysis, the ratio of contribution from the flux flow to the total electric field is estimated. A discussion will be given on a relationship between the pinning parameters used in the flux creep-flow model and the fitting parameters used in the percolation flow model, which describe the E-J characteristics phenomenologically. Moreover, a value of U_0 is estimated from an ohmic E-J characteristic measured in the range of TAFF state with the flux creep theory, and the result is compared with the values estimated by other methods.

3.1 Flux creep-flow model

We will here explain the flux creep-flow model [17], in which the distribution of flux pinning strength and the thermal motion of flux lines are taken into account.

Assume a virtual case in which the thermally activated flux creep does not take place. Using the critical current density in this case J_{c0}, the electric field due to the flux flow, E_{ff}, is given by

$$\begin{aligned} E_{ff} &= 0; && j \leq 1, \\ &= \rho_f(J - J_{c0}); && j > 1, \end{aligned} \tag{3.1}$$

where $j = J/J_{c0}$ and ρ_f represents the flow resistivity, which is estimated as $\rho_f = (B/B_{c2})\rho_n$ using the Bardeen-Stephan model[4]. In high-temperature superconductors the normal resistivity ρ_n varies with temperature as $\rho_n = (T/T_c)\rho_n(T_c)$.

In the actual case, the electric field is generated even at j lower than 1. This is due to the flux creep as shown in section 1.2.2. From Eq. (1.9), the electric field is given by

$$E_{cr} = Ba_f\nu_0 \exp\left[-\frac{U(j)}{k_B T}\right]\left[1 - \exp\left(-\frac{\pi U_0 j}{k_B T}\right)\right]; j \leq 1$$

When $j > 1$, it is considered that the contribution of the flux creep is a constant and we assume the value is given with $j = 1$. In this case, since the activation energy U is zero, we have

$$E_{cr} = Ba_f\nu_0\left[1 - \exp\left(-\frac{\pi U_0}{k_B T}\right)\right]; \qquad j > 1$$

Therefore, under the flux creep, the current-voltage characteristics is estimated by the pinning potential U_0 and the virtual critical current density J_{c0}.

Since the electric field is contributed by the flux creep and the flux flow, here we assumed that the total electric field is approximately given by

$$E = (E_{cr}^2 + E_{ff}^2)^{1/2}. \tag{3.3}$$

In fact, when $j < 1$, E is only E_{cr} of the electric field due to the flux creep. While, when $j \gg 1$, E_{ff} has a majority in it. Therefore, this approximate estimate is considered to be good.

While, it is generally well-known that the J_{c0} in an oxide superconductor is widely distributed. This includes the essential distribution of the pinning force. Moreover, in fact it is considered to include the influence of the weak links and the sausaging and so on. The weak links make J_{c0} decreased increasing a temperature. The sausaging is that the thickness of the fine filaments is not uniformity. In this paper we use the practical distribution of the pinning force. Therefore, we simply assume that the only A in Eq. (1.47) is distributed as

$$f(A) = K\exp\left[-\frac{(\log A - \log A_m)^2}{2\sigma^2}\right], \tag{3.4}$$

where A_{m} is the most probable value, K is a constant determined by the condition of normalization and σ^2 is a constant representing the degree of deviation.

Therefore, if the parameters is given, the E-J curves in the total of a superconductor can be estimated as

$$E(J) = \int_0^\infty E f(A) \mathrm{d}A. \tag{3.5}$$

The pinning parameters and σ^2 are determined so that a good fit is obtained between the experimental and theoretical values of the critical current density $J_{\mathrm{c}}(B, T)$.

3.2 Comparison between the experimental and theoretical E-J characteristics.

Figures 3.1 $\sim$ 3.5 show the E-J curves at 40 $\sim$70 K evaluated from the four probe method (top) and the magnetization relaxation method (bottom). The electric field in the relaxation method is of the order of 10^{-10} V/m and is 6 to 7 orders of magnitude lower than the four probe method. Therefore, the E-J characteristics are evaluated over a quite wide range of the electric field.

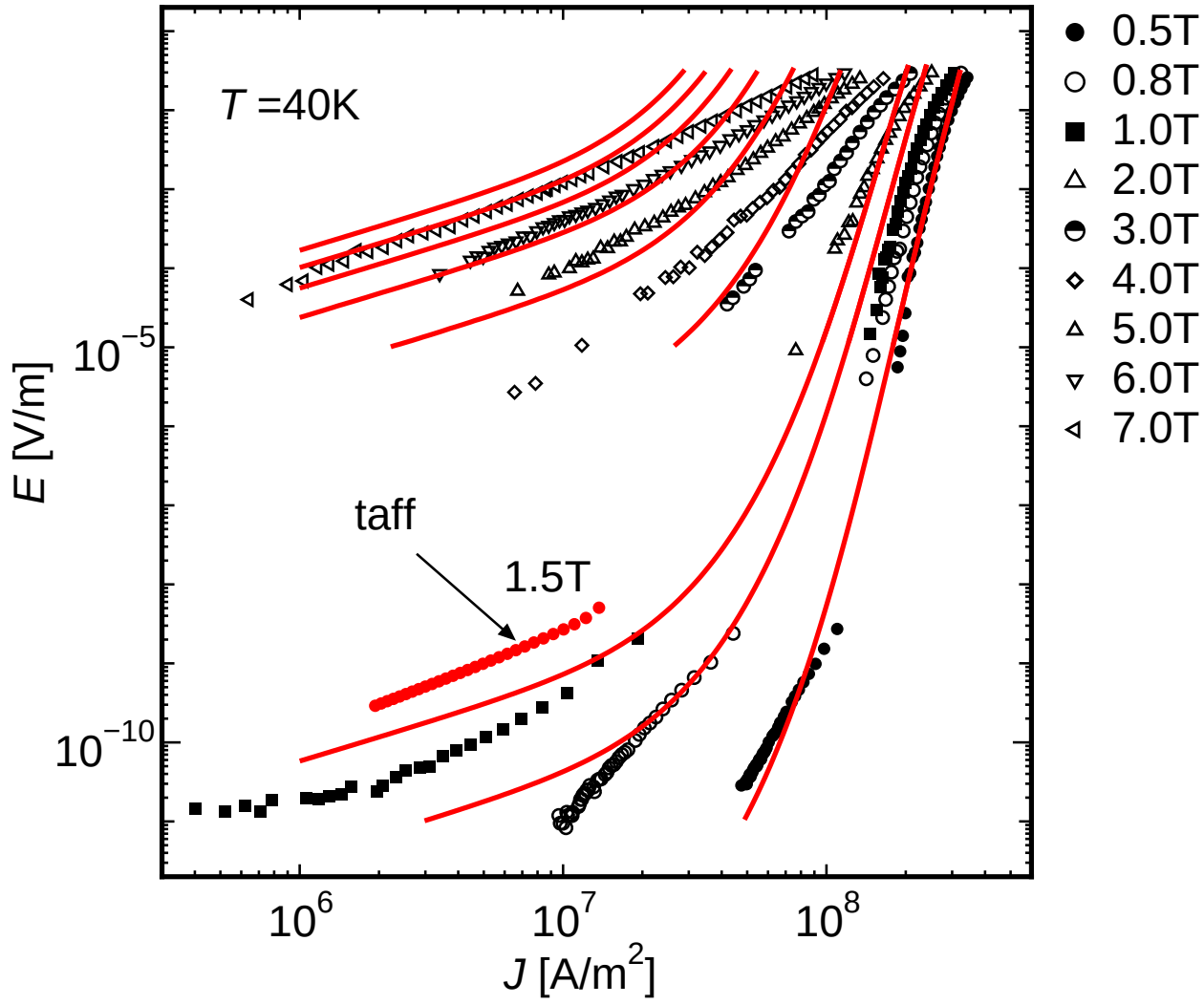

Fig. 3.1. Comparison of E-J curves between experiment (symbols) and theory (lines) at 40 K.

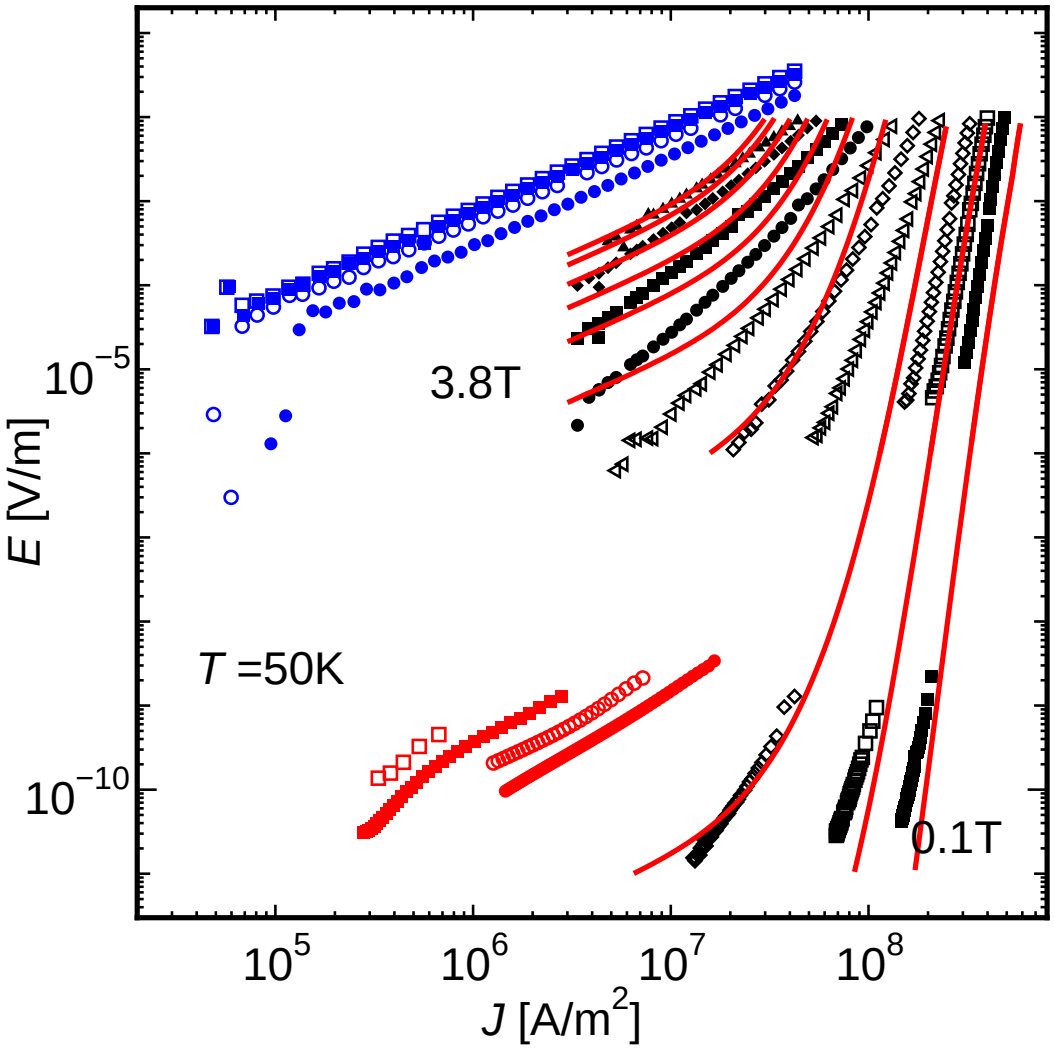

Fig. 3.2. Comparison of E-J curves between experiment (symbols) and theory (lines) at 50 K.

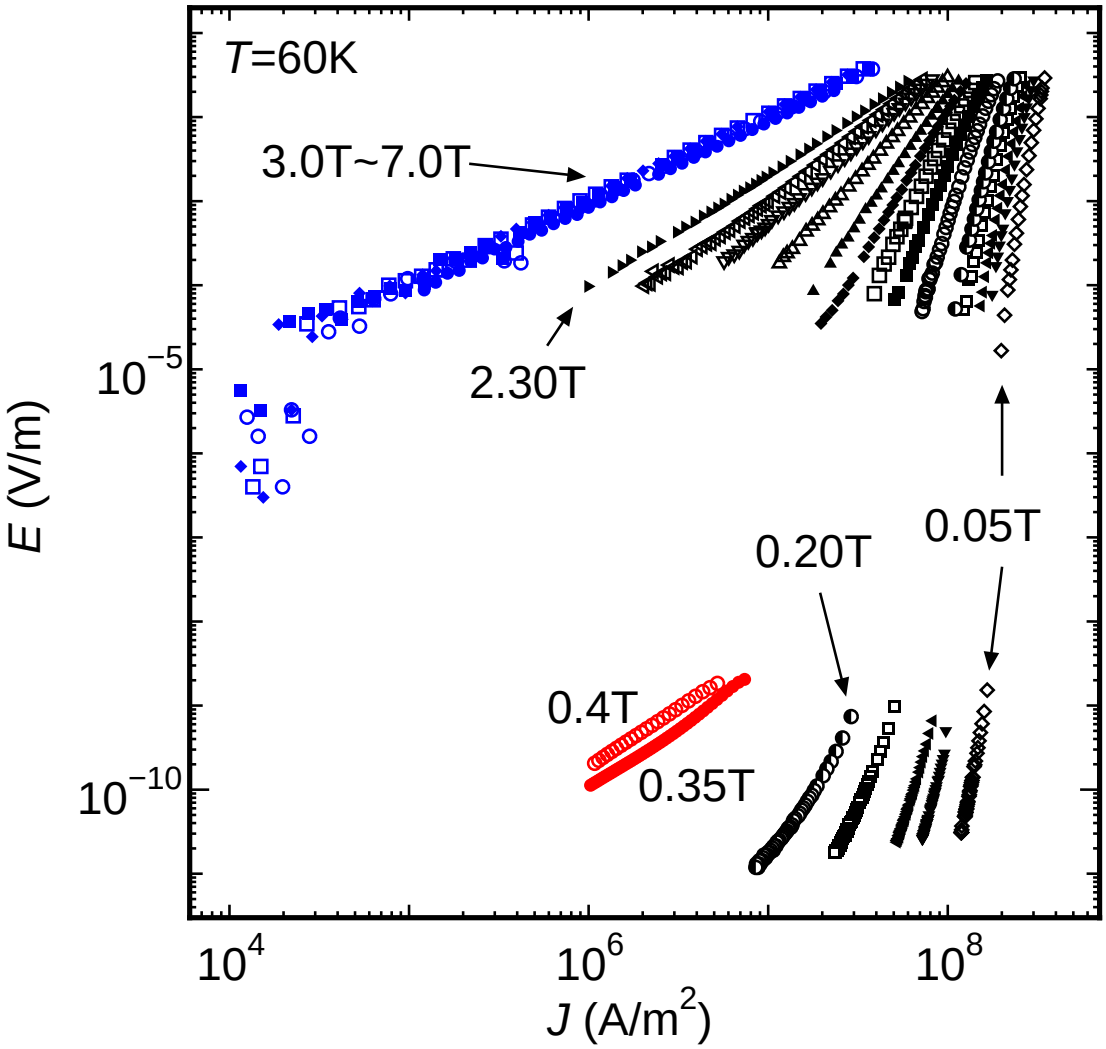

Fig. 3.3. Comparison of E-J curves between experiment (symbols) and theory (lines) at 60 K.

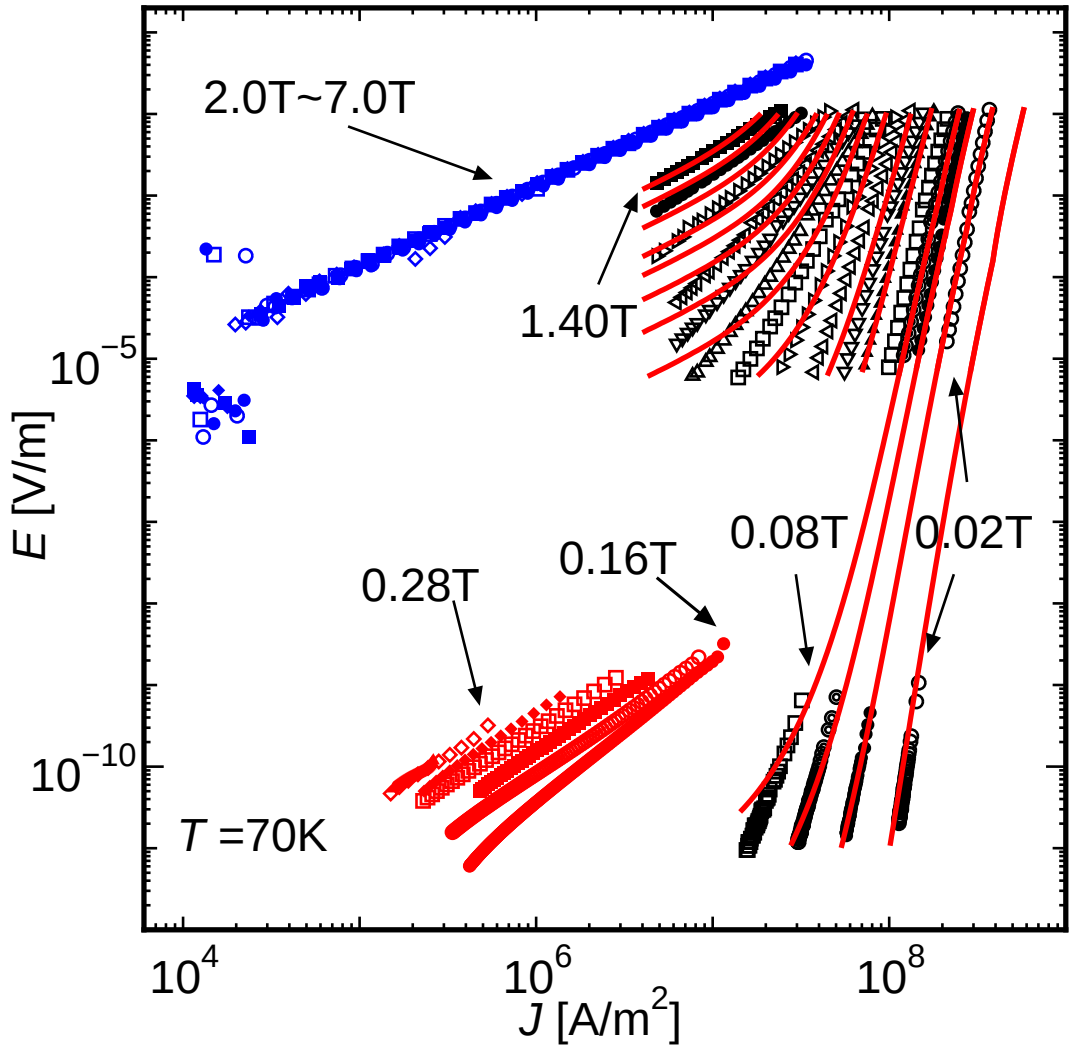

Fig. 3.4. Comparison of E-J curves between experiment (symbols) and theory (lines) at 70 K.

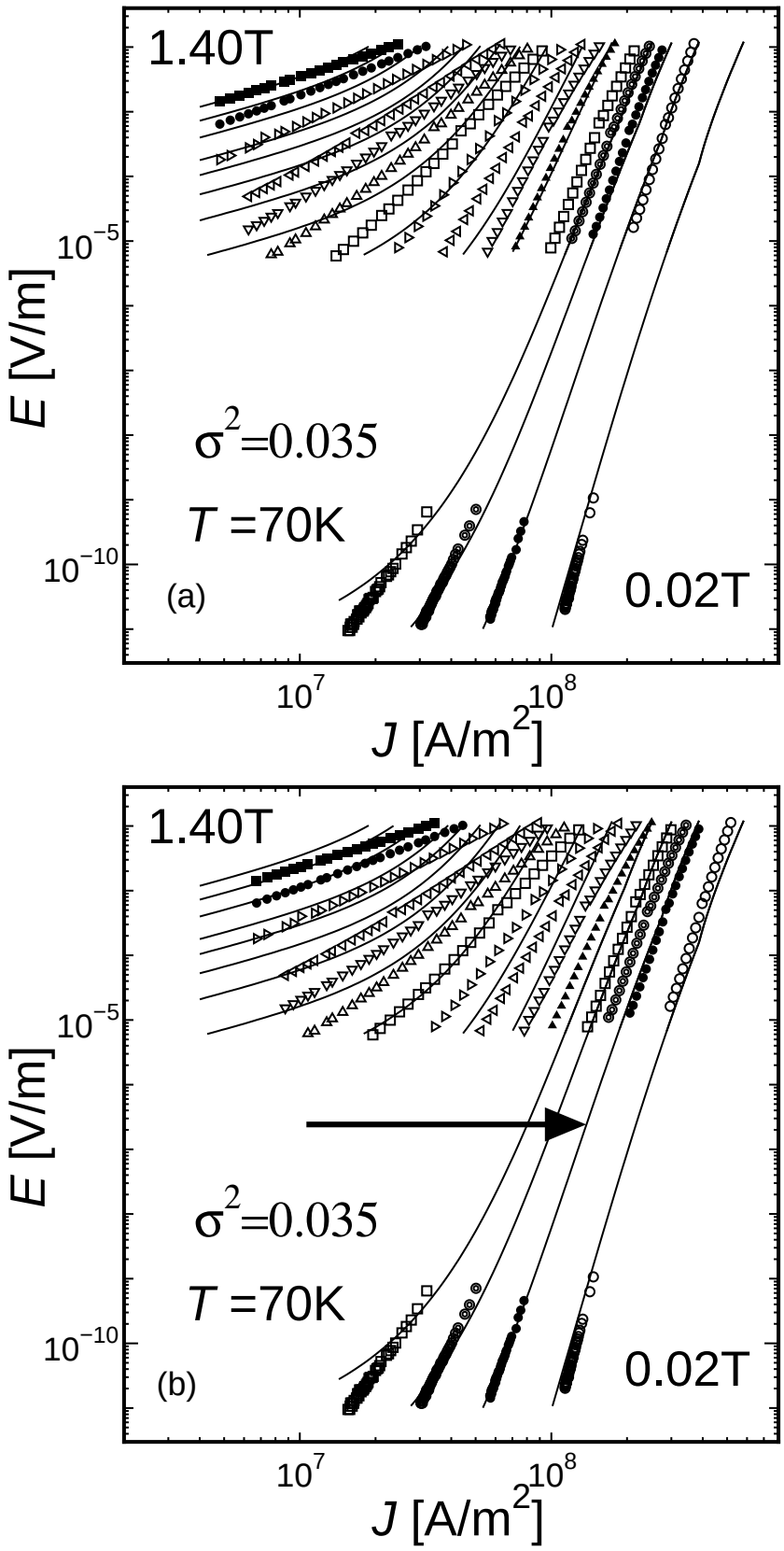

Fig. 3.5. Comparison of E-J curves between experiment (symbols) and theory (lines) at 70 K. Experimental results are obtained by four probe method (top) and the magnetization method (bottom). (a) represents original data and E-J caves of the four probe method are displaced by a factor 1.4 in the direction of higher J in (b).

The solid lines in Fig. 3.5(a) are the theoretical E-J curves at 70 K which will be argued later. As seen in this figure, the deviation between the experimental and theoretical results is different between the high electric field range and the low electric field range. This is considered to be caused by a sausaging of superconducting filaments. That is, J in the magnetization method is an average value, while J in the four probe method is mostly determined by narrow regions of filaments. Usually the latter is larger than the average value. Actually, if E-J curves of the four probe method are displaced by a factor 1.4 in the direction of higher J as shown in Fig. 3.5(b), the curves in the two regions coincide with each other. In fact, the difference of factor 1.4 can be explained by the observed distribution of superconducting filaments.

Values of $A_{\rm m}$, m and γ listed in Table 3.1 are used in the numerical calculation in a wide range of temperature and magnetic field. According to Eq. (1.43), g^2 depends on E as well as on B and T. In this study, for simplicity, the E in Eq. (1.43) is considered as a constant of $E = 10^{-10}$ V/m, which is representatively determined by the electric field criterion, $E_{\rm c}$, in the range of relaxation measurement. For example, the theoretical value of g^2 is 1.39 at $T = 70$ K and $B = 0.3$ T. Here, the theoretical g^2 equation in Eq. (1.43) is derived for the region far from the TAFF state. Strictly speaking, it is not self-consistent that the theoretical expression of g^2 is used in the vicinity of TAFF state. However, this theoretical value of g^2 is used in this study.

On the other hand, σ^2 is used as a fitting parameter at each temperature with assuming the independence of B and E, and the temperature dependence is shown in Fig. 3.6. As shown in Figs. 3.1 $\sim$ 3.5, the theoretical results can explain the experimental results in wide range of the electric field. Therefore, the assumed parameters in this analysis seem to be reasonable.

Table 3.1. Parameters used in the numerical calculation.

$A_{\rm m}$	m	γ
9.0×10^8	2.0	0.51

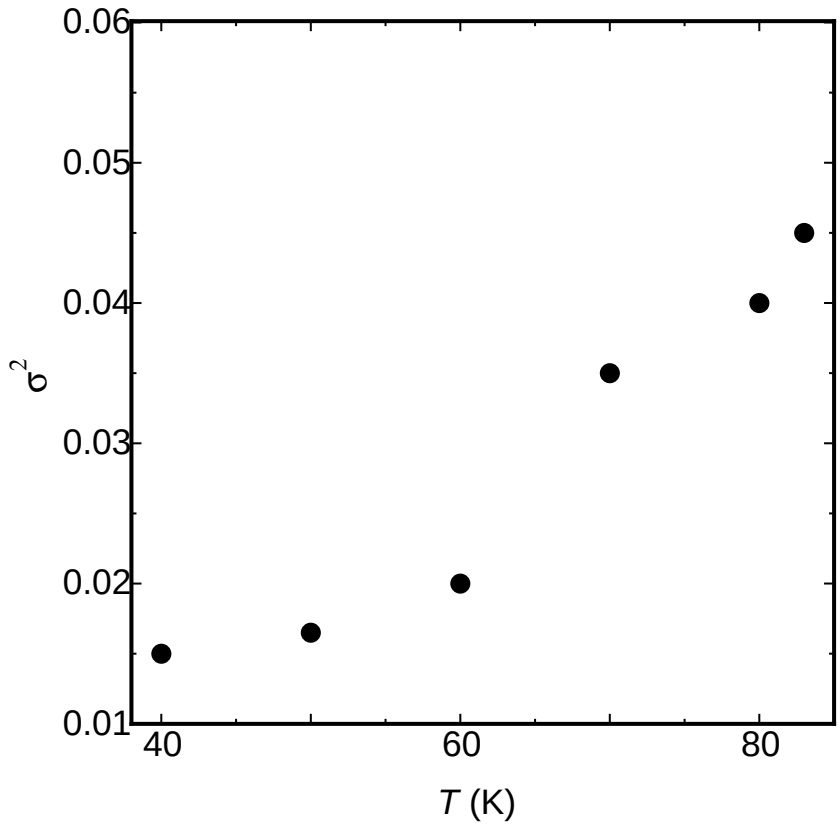

Fig. 3.6. Temperature dependence of σ^2.

The observed electric fields are smaller than the theoretical ones in a range of high electric field and high magnetic field. This deviation comes from the sharing flow of current to the silver sheath in experiment. In the analysis the parallel circuit model of superconductor and silver matrix was used. However, the results did not change largely even by consideration of sharing current flow to the matrix. The reason for this deviation is not clear now.

Thus, it can be said that the flux creep-flow model can approximately describe the E-J characteristics in wide ranges of temperature, magnetic field and electric field. This shows that the thermal depinning is the basic mechanism which determines the E-J characteristics.

Fig. 3.7 shows the magnetic field dependence of the pinning force density $F_{\rm p}$ at 70 K defined at (a) $E = 1.0 \times 10^{-4}$ V/m and (b) $E = 1.0 \times 10^{-10}$ V/m in the four probe and magnetization methods, respectively. It is seen that the value of $F_{\rm p}$ and the peak magnetic field have larger values at higher electric field. This suggests that the effect of the flux creep is very large in two-

dimensional superconductors such as Bi-2223. This is caused by the weak pinning force and the small transverse bundle size due to a poor superconductivity in the block layer.

Fig. 3.6 shows that the distribution width of J_c increases with temperature. When the temperature approches T_c, the distribution of T_c is larger than that of the low temperature. This contributes the increased width of J_c with temperature. This tendency is consistent with the usual temperature dependence of n-value by the flux creep, since n which characterizes the E-J property as $E \propto J^n$ becomes usually smaller if the distribution width of J_c increases with temperature.

Although the present theoretical model approximately explains the observed E-J characteristics, the details cannot be explained. That is, as the current density J becomes smaller, the theoretical n takes on much smaller value than the experimental value. The reason for this deviation is considered to be attributed to the expression of g^2 at low current densities. That is, the electric field dependence of g^2 was disregarded. In addition, Eq.(1.43) can be applied to the region far from the TAFF(Thermally Activated Flux Flow) state. However, the theoretical prediction shows a typical TAFF behavior as can be seen in Fig. 3.5. Thus, a self-consistent theoretical expression of g^2 should be obtained.

On the other hand, the finite ohmic resistance given by TAFF model is not predicted by the collective flux-creep model by Feigel'man *et al.*[18] in the range of the flux creep. Their theory assumes a nonlinear J dependence of the activation energy, such as $U \sim J^{-\mu}$. In this assumption the activation energy diverges when $J \to 0$. Therefore, the collective flux-creep model shows the same behavior in the glass state of flux lines as in the vortex glass-liquid transition model[19, 20]. That is, the electric field is predicted not to be generated in the range of sufficiently small current density. As a result, the E–J characteristics convex upward should be maintained in a whole range of the magnetic field smaller than the transition field. As is seen in Fig. 3.5, the experimental E–J curves show a typical convex upward behavior in the glass state at low magnetic fields in the range of high electric field. On the other hand, the curves are obviously convex downward like those in the liquid state

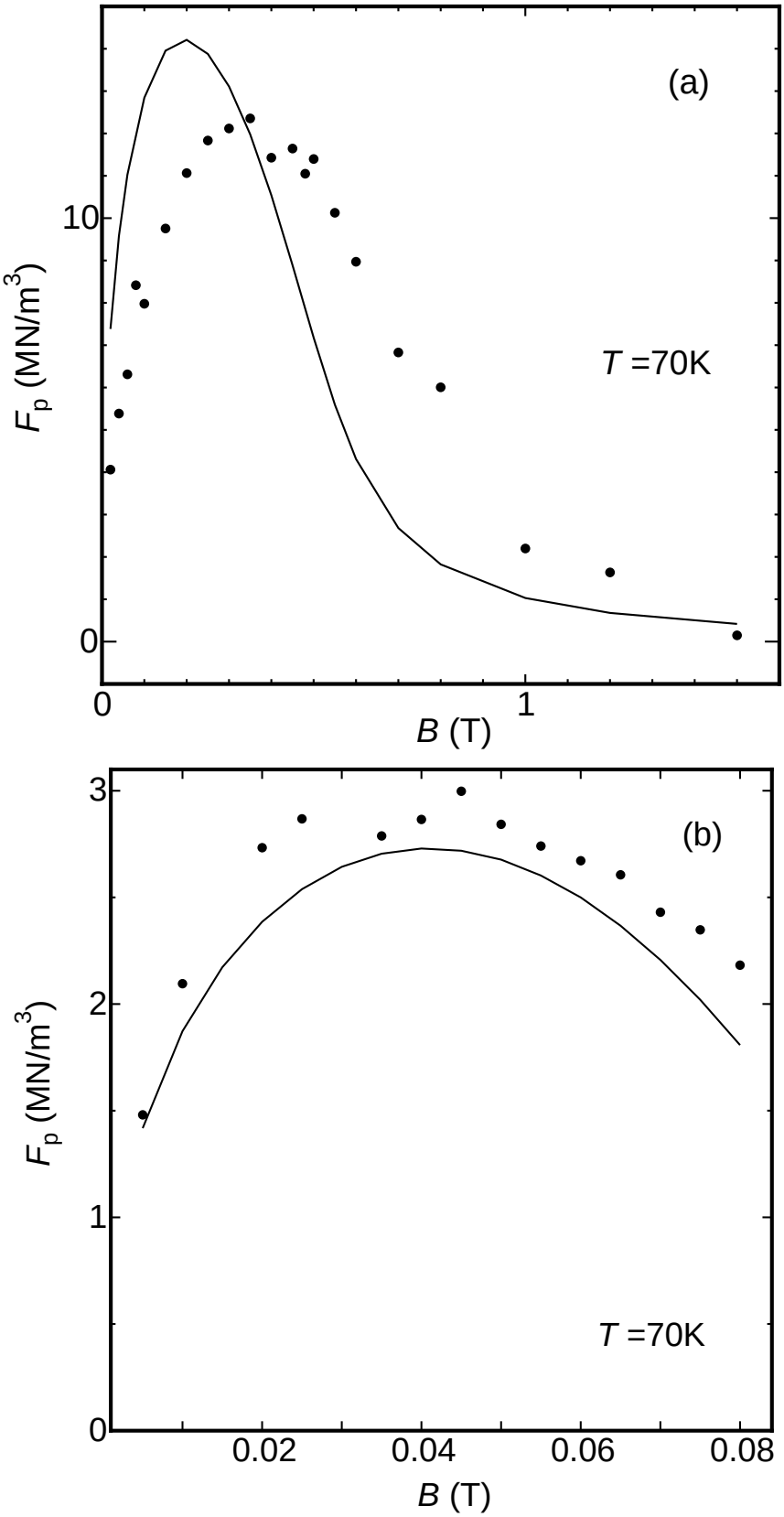

Fig. 3.7. Pinning force density at 70 K defined at (a) high and (b) low electric fields. Symbols and lines show experiment and theory, respectively.

in the range of very low electric field. Hence, this is contradictory to both the collective flux-creep model and the vortex glass-liquid transition model. Such a tendency was also shown in the experimental results of Nakamura *et al.*[7] for an Y-123 thin film, as mentioned in section 1.4.3.

According to the theory on the flux bundle size in which the irreversible thermodynamic principle is considered[21], the number of flux lines inside the flux bundle is given by Eq. (1.43) at the electric field strength E. Hence, the flux bundle size is predicted to become larger as E becomes smaller. Thus, the E–J characteristics convex upward is derived. However, the flux bundle size is finite, and it does not diverge. That is, the flux bundle size is limited by $g_e a_f$ for the perfect flux line lattice. In usual flux line lattices imperfections are included and the flux bundle size is much smaller than this value. It should be noted that the practical flux bundle size is different from the elastic correlation length of the flux lattice which diverges at the vortex glass-liquid transition field. This is an essential point that this theory is different from the theory of Feigel'man *et al.* The elastic correlation length gives only the maximum of the flux bundle size. That is, the elastic correlation length itself does not change with E as assumed by Feigel'man *et al.* but is a constant, while the flux bundle size changes as predicted by the law of the irreversible thermodynamics.

In the present analysis, the electric field dependence of g^2 is not considered. If this dependence is taken into account, g^2 becomes larger as the electric field becomes smaller, resulting in a smaller effect of the flux creep. Therefore, the n-value is predicted to become large, and the agreement between theoretical and experimental results will be better.

The other reason is considered about the deviation of the E–J characteristics at low current densities. The generated electric field is strongly influenced by the percolation process of flux lines. Therefore, the magnetic field dependence of the percolation process is different by the range of the electric field due to the flux creep or the flux flow. That is, it is considered that the distribution given by Eq. (3.4) depends on the range of the electric field.

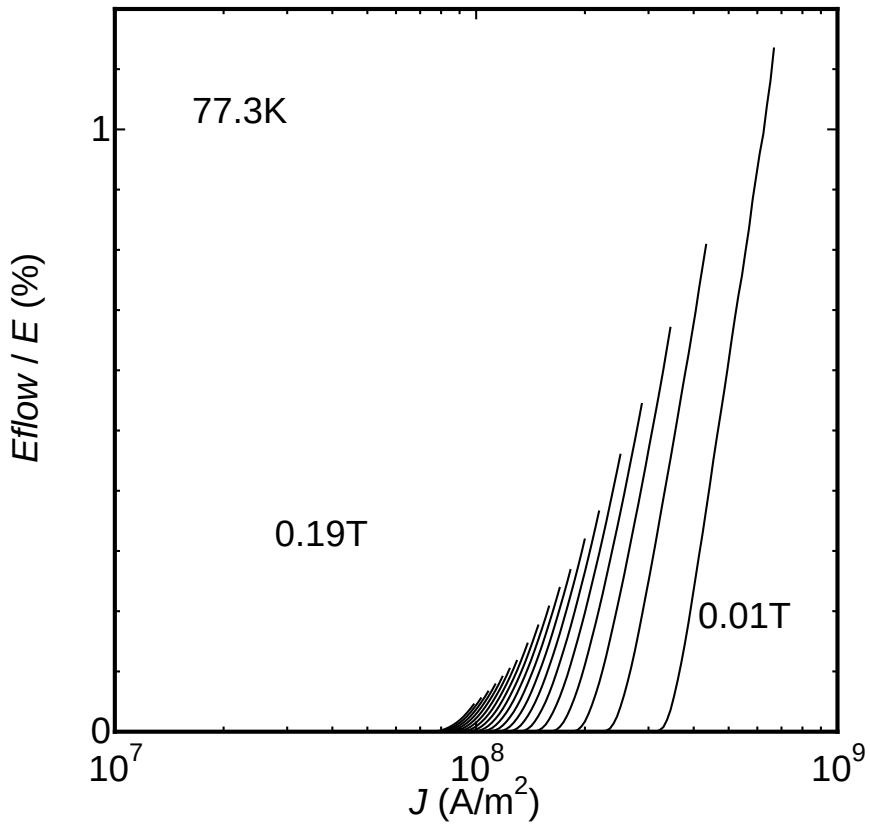

Fig. 3.8. Ratio of contribution of flux flow to the total electric field predicted by the flux creep-flow model at 77.3 K. Magnetic field is varied from 0.01 T to 0.19 T with a step of 0.01 T.

3.3 Ratio of contribution of flux flow to the total electric field

The induced electric field is composed of the two components of flux creep and flux flow. Figure 3.8 shows the ratio of flux flow component to the total electric field at 77.3 K. For example, the ratio of the flux flow component is about 1% at 0.01 T. The ratio becomes smaller with decreasing temperature. Hence, the most of electric field is caused by the flux creep even in the electric field range of resistive measurement. This result is consistent with the fact that the mechanism of flux creep generally explains various phenomena such as the critical current density, the irreversibility field and so on.

It is known that the E-J curves measured by the four probe method can easily be calculated by the percolation flow model, in which the flux creep

is approximated by an equivalent flux flow. This approximation is done by making the pinning potential shallow as in Fig. 1.15. However, in the creep region of a very low electric field such as 10^{-10} V/m, the theoretical prediction deviates from experiment due to a part of flux creep which was neglected. Therefore, an extensive percolation flow model which takes account of the flux creep was proposed[15]. In addition, a new attempt frequency ν_0' is assumed as a fitting parameter instead of ν_0 in Eq. (1.22), and a value of the order of 10^7 Hz is used to explain experimental results at low electric fields[15].

The attempt frequency, ν_0, is theoretically derived as in Eq. (1.22). Its value is of the order of 10^{10} Hz and is about 3 orders of magnitude higher than ν_0' in the extensive percolation flow model. Since the potential barrier is given by $U_1 + \Delta U$ as illustrated in Fig.1.1(b), the electric field due to the flux creep is expressed as

$$E = Ba_{\mathrm{f}}\nu_0 \exp\left(-\frac{U_1}{k_{\mathrm{B}}T}\right)\exp\left(-\frac{\Delta U}{k_{\mathrm{B}}T}\right). \tag{3.6}$$

Hence, ν_0' is formally given by

$$\nu_0' = \nu_0 \exp\left(-\frac{U_1}{k_{\mathrm{B}}T}\right). \tag{3.7}$$

This shows that ν_0' is much smaller than ν_0. The difference of 3 orders of magnitude can be explained by assuming $U_1/k_{\mathrm{B}} = 534$ K at 77.3 K. This value seems to be reasonable for Bi-2223 superconductor.

Here, the results of the two theoretical models are compared. In the first place, the theoretical E-J curves of the flux creep-flow model are adjusted to fit the experimental curves. Secondly, the theoretical results of percolation flow model are also adjusted to fit the experimental results. Then, these two theoretical results are directly compared in Fig. 3.9. A fairly good agreement was obtained between the two models. Therefore, it can be concluded that the percolation flow model is consistent with the flux creep-flow model. This means that the flux creep-flow model can give a theoretical foundation of the percolation flow model. Namely, J_{cm}, which is merely a fitting parameter in the percolation flow model, can be explained using J_{c0} which can be estimated on the basis of material parameters. Therefore, this gives the theoretical proof for the percolation flow model. The last problem is to check the simple

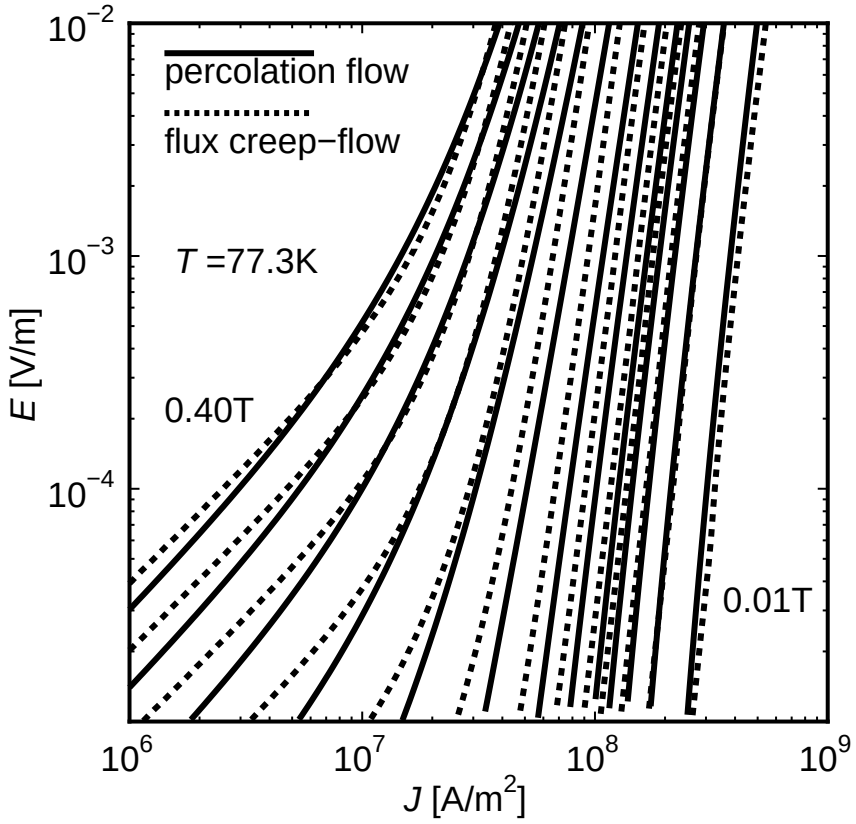

Fig. 3.9. Comparison of E-J theoretical curves between the flux creep-flow model (dotted lines) and the percolation flow model (solid lines) at 77.3 K.

assumption on the proportionality between ΔU and $J_{\rm cm}$ in the range of low electric field.

3.4 Pinning potential U_0

The pinning potential, U_0, is an important parameter to determine the irreversibility field and the relaxation rate of the superconducting current due to the flux creep as mentioned in sections 1.2.2 and 1.2.3, as well as the E-J characteristics.

Here, a new method of estimation of U_0 is proposed with the aid of the flux creep theory with $J_{\rm c0}$ evaluated in section 3.2.

As shown in Figs. 3.10 and 3.11, the symbols show the E-J characteristics obtained by the relaxation measurement with the SQUID magnetometer at magnetic fields close to the irreversibility fields. It is found that the E-J

characteristics in the range of sufficiently small J are close to those expressed as $E \propto J$ in the TAFF state. The E-J characteristics are shown by red symbols in Fig. 3.1∼3.4. The E-J characteristics in the TAFF state are described as Eq. (1.24). The solid lines in Fig. 3.1∼3.4 show Eq. (1.24), where U_0 is used as a fitting parameter. In the above, it is assumed that J_{c0} is not distributed but is given by the most probable value:

$$J_{c0} = A_m \left[1 - \left(\frac{T}{T_c}\right)^2\right]^m B^{\gamma-1} \left(1 - \frac{B}{B_{c2}}\right)^\delta, \tag{3.8}$$

Then, U_0 can be estimated. The evaluated values of U_0 are shown as black symbols in Figs. 3.12∼3.16. As the magnetic field increases, U_0 decreases. The dependence is not strong.

U_0 was also estimated using the other methods. Here, some of other methods are briefly introduced in the following, in order to compare with the above new method.

(1) Analysis of the observed irreversibility field

When observed results of the irreversibility field and the irreversibility temperature are substituted into Eq. (1.27), U_0 can directly estimated. The open symbols in Fig. 3.17 show observed irreversibility fields which are determined with $E_c = 10^{-10}$ V/m and $\Delta J_c = 10^7$ A/m^2 for the criterion of J_c.

(2) Theoretical analysis of the E-J characteristics

U_0 can also be theoretically estimated from Eq. (1.24). For simplicity, the most probable value of J_{c0} of Eq. (3.8) is used.

(3) The E-J characteristics in the range of TAFF state using the four probe method

Using the four probe method, the ohmic E-J characteristics in the TAFF state are measured. Equation (1.25) leads to

$$\log \rho \simeq -\frac{U_0}{k_B T} + \log \rho_0. \tag{3.9}$$

Hence, U_0 can be estimated from the slope of the relationship of $\log \rho$ vs $1/T$, as mentioned in section 1.2.2.

Figs. 3.12∼3.16 show comparison among the results obtained by the above methods. The open symbols and solid lines are obtained from the analysis of the observed irreversibility field in (1) and the E-J characteristics in (2), respectively.

Although a slight deviation is seen among three methods, they are approximately consistent. Therefore, the value of U_0 using the new method seems to be reasonable. However, this deviation is considered to be attributed to the neglected distribution of J_{c0}.

Here, the irreversibility field is considered again. All symbols and lines in Fig. 3.17 are determined wtih $E_c = 10^{-10}$ V/m and $\Delta J_c = 10^7$ A/m^2. The open symbols show observed results. The dotted line is theoretical result estimated from the E-J characteristics in which the distribution of J_{c0} is taken into account. The theoretical result can explain the observed result. On the other hand, the theoretical irreversibility field estimated from Eq. (1.49) with the most probable value of J_{c0} is shown by the solid line in the figure. A large deviation is seen between the dotted line and the solid line. The reason for this deviation is also considered to be the distribution of J_{c0}.

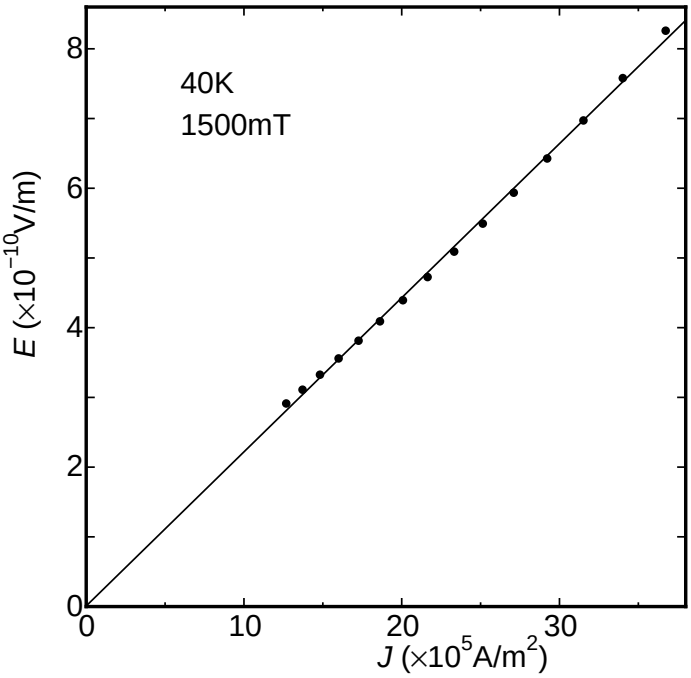

Fig. 3.10. Comparison of experimental(symbol) and theoretical(line) E-J curve at 40.0 K and 1500 mT in the TAFF state.

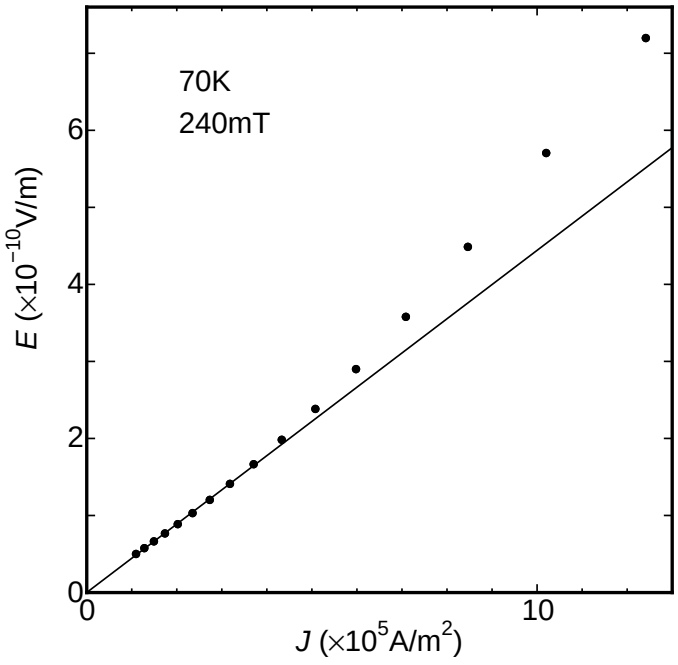

Fig. 3.11. Comparison of experimental(symbol) and theoretical(line) E-J curve at 70.0 K and 240 mT. The solid line lines show the curve in TAFF state.

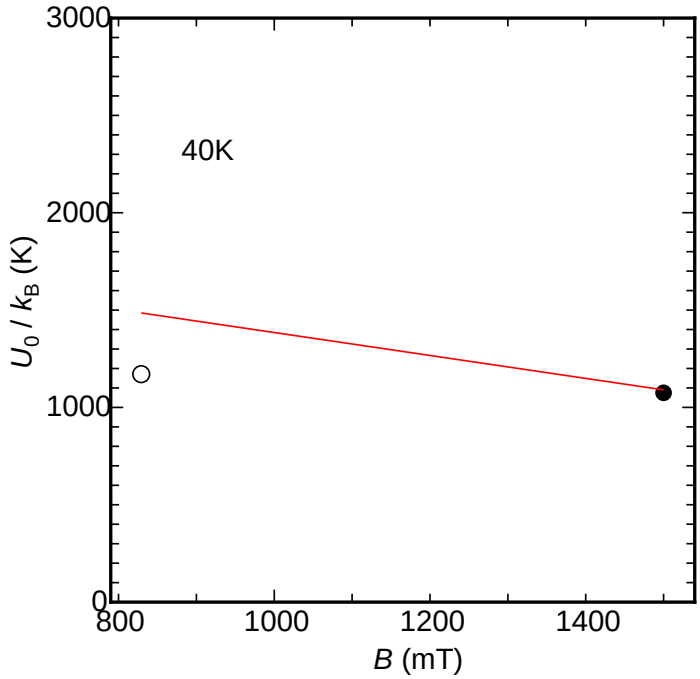

Fig. 3.12. Experimental(solid symbol) and theoretical(line) pinning potential at 40.0 K. Open symbol shows the pinning potential estimated from the irreversibility field.

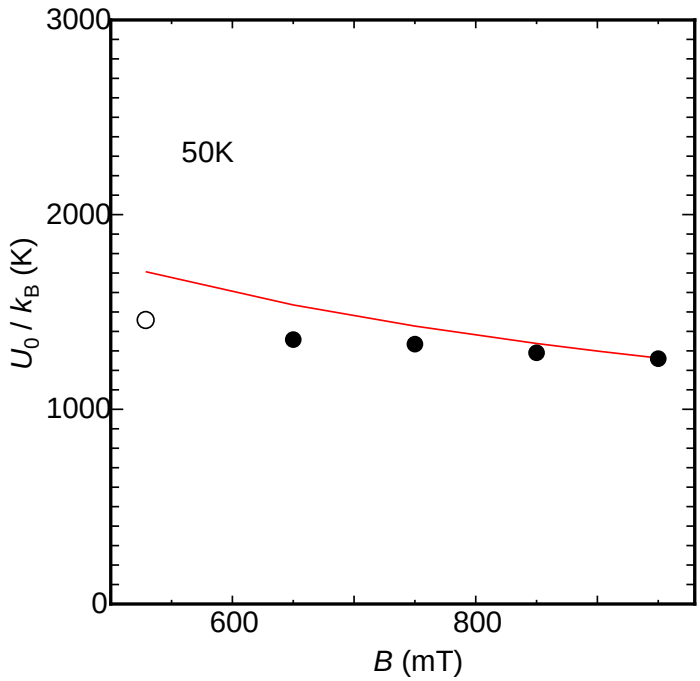

Fig. 3.13. Experimental(solid symbol) and theoretical(line) pinning potential at 50.0 K. Open symbol shows the pinning potential estimated from the irreversibility field.

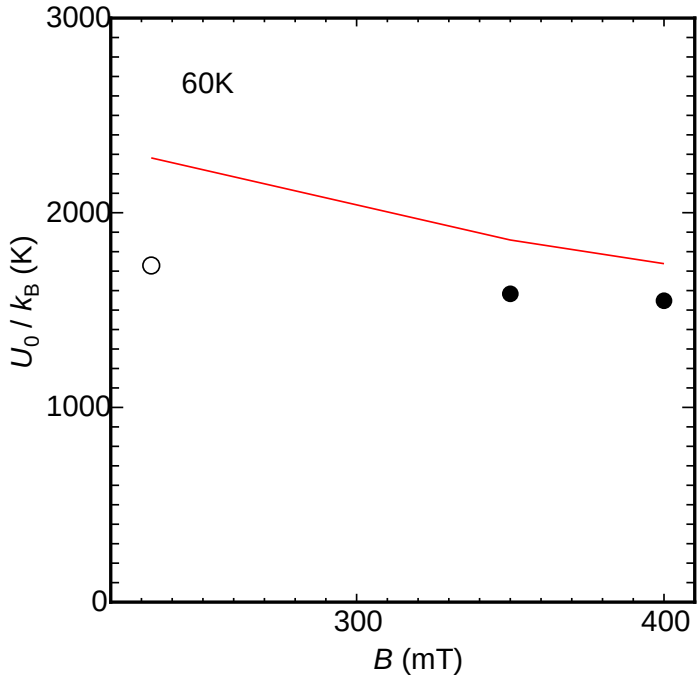

Fig. 3.14. Experimental(solid symbol) and theoretical(line) pinning potential at 60.0 K. Open symbol shows the pinning potential estimated from the irreversibility field.

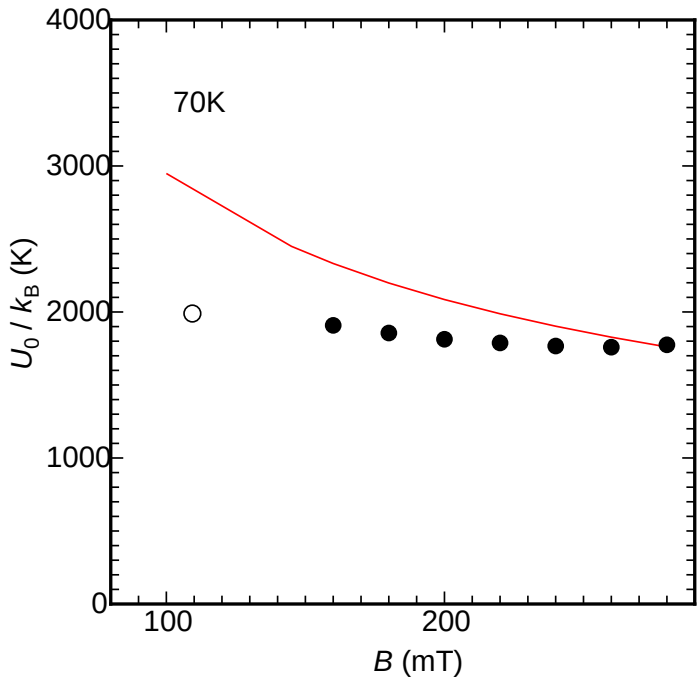

Fig. 3.15. Experimental(solid symbol) and theoretical(line) pinning potential at 70.0 K. Open symbol shows the pinning potential estimated from the irreversibility field.

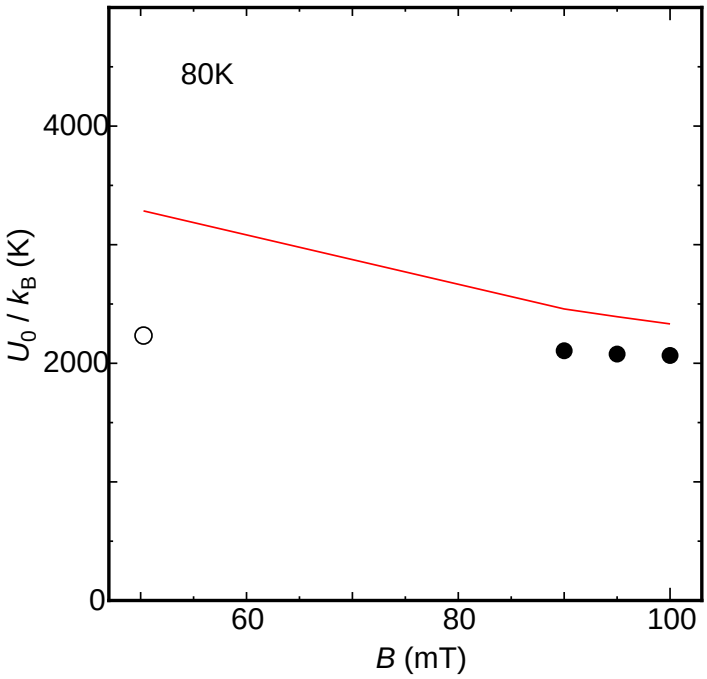

Fig. 3.16. Experimental(solid symbol) and theoretical(line) pinning potential at 80.0 K. Open symbol shows the pinning potential estimated from the irreversibility field.

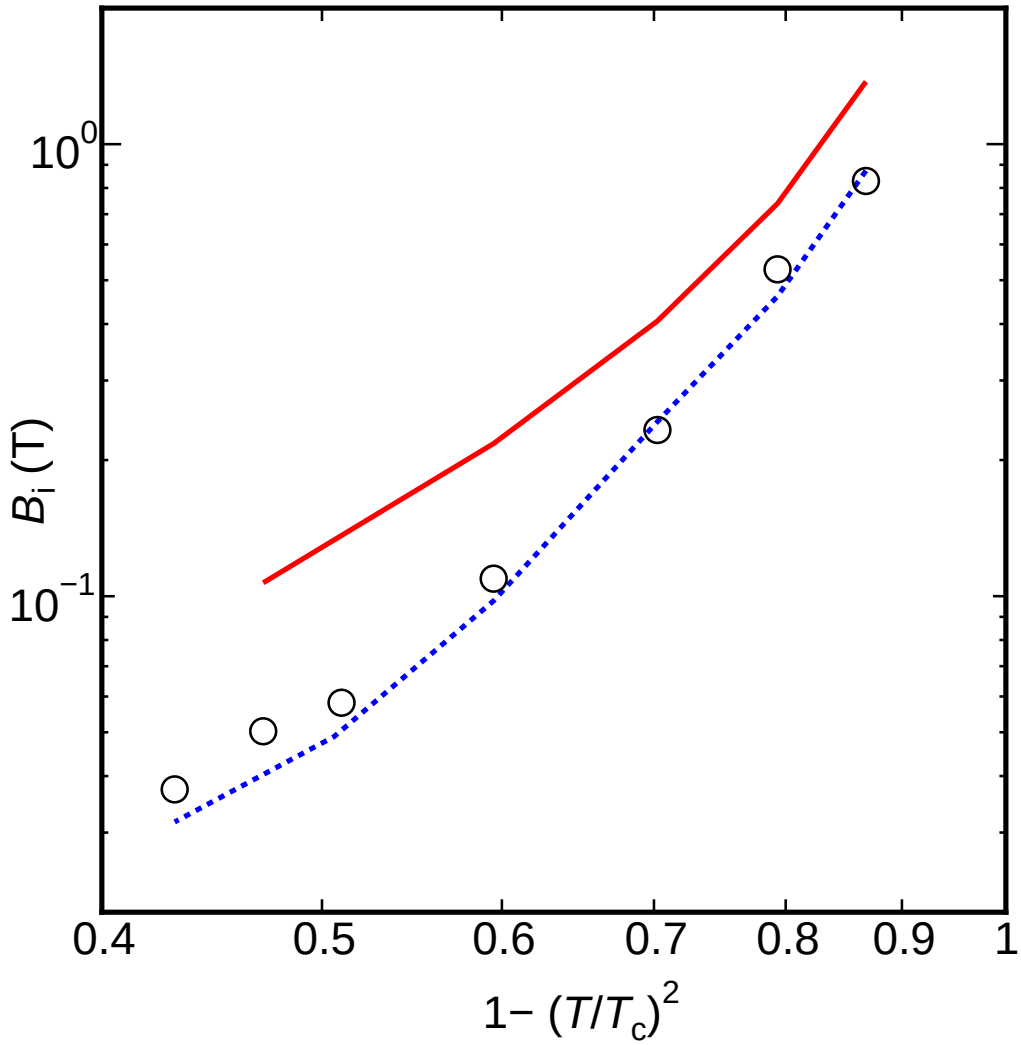

Fig. 3.17. Irreversibility field: open symbols are observed results. solid and dotted lines are theoretical results for the most probable value and the distribution of J_{c0}, respectively.

Chapter 4

Conclusions

4.1 Summary

In this study, the E-J characteristics are evaluated in a wide range of the electric field and the pinning potential U_0 is estimated for a superconducting Bi-2223 silver-sheathed tape. The following results are obtained.

- The E-J characteristics are approximately explained by the flux creep-flow model in wide ranges of temperature, magnetic field and electric field. Therefore, it is concluded that the thermal depinning is the basic mechanism which determines the E-J characteristics. This gives the theoretical proof for the percolation flow model in which the characteristics are expressed by an equivalent flux flow in the range of a significant flux creep.

- The difference of the characteristics between the four probe and magnetization methods can be attributed to the effect of filament sausaging.

- As the electric field becomes small, the value of $F_{\rm p}$ in Bi-based superconductor decreases drastically. This suggests that the effect of the flux creep is very large in two-dimensional superconductors. This is ascribed to a poor pinning force and a small transverse bundle size, the both of which are caused by the poor superconductivity in the block layer.

- The E–J characteristics show the flux-glass like state in the range of high electric field, while those behave like the liquid state in the range of very low electric field. This is not consistent with the prediction of

the collective flux creep-model by Feigel'man *et al.* and the glass-liquid transition theory. On the other hand, the principle of the irreversible thermodynamics for the flux bundle size is considered to be essential, and theory predicts that, when the current density is decreased, a finite ohmic electric resistivity is generated similarly to the TAFF model.

- The large deviation is observed between experimental results and theoretical results at low current densities. One of the reasons is considered to be a deviation of g^2 for the theoretical expression at low current densities. Another reason is that the magnetic field dependence of the percolation property is different by the observed electric field, and the distribution such as Eq. (3.4) is different by the observed electric field, too.

- It is found that most of the electric field is caused by the flux creep even in the range of the usual resistive measurement. This result is consistent with the fact that the mechanism of flux creep generally explains various phenomena such as the critical current density, the irreversibility field and so on.

- A difference of the attempt frequency of flux bundle between the flux creep-flow model and the extensive percolation flow model can be explained by a difference of assumed pinning potential.

- The flux creep-flow model can give a theoretical foundation of the percolation flow model in the electric-field range of usual resistive measurements.

- It is found that the E-J characteristics observed using a relaxation method in the vicinity of the irreversibility field are close to those in the TAFF state.

- It is found that U_0 can be quantitatively estimated by comparing the observed and the theoretical E-J characteristics in the TAFF state. Although a slight deviation is seen due to the distribution of J_{c0}, the value of U_0 is considered to be reasonable from comparison with those obtained by other methods.

- A large deviation is seen between the irreversibility field estimated using the most probable value of J_{c0} and the irreversibility field in which the distribution of J_{c0} is taken into account. This shows that the distribution of J_{c0} affects the irreversibility field strongly.

Appendix A

Appendix

A.1 Estimation of the E-J characteristics using a magnetization method

We suppose a rectangular superconducting filament with a width w, a length l ($\gg w$) and a thickness d as shown in Fig. A.1. The $x-$, $y-$ and $z-$ axes assumed in the directions of the width, the length and the thickness. It is supposed that an external magnetic field of a sufficient magnitude $B_{\rm m}$ was first applied to the filament along the z-axis, and then, decreased to a desired value for the measurement $B_{\rm e}$, so that the filament could be in the critical state. The Bean model, in which the current density J is a constant, is assumed for the shielding current induced inside the filament. Therefore, the flux distribution in the critical state is shown in Fig. A.2. The corresponding flux distribution in the x-z plane and the current distribution (along the y axis) are shown in Fig. A.3.

The path of the current in the filament which flows on point, Q($x,\ y,\ z$), is supposed. As seen in this Fig. A.4, the path C is given by a rectangle which is composed of four apexes of P$_1$($x,\ x+(l-w)/2,\ z$), P$_2$($-x,\ x+(l-w)/2,\ z$), P$_3$($-x,\ -x-(l-w)/2,\ z$) and P$_4$($x,\ -x-(l-w)/2,\ z$). If $S(x)$ is an area of the section surrounded by the closed loop, C, a magnitude of a magnetic moment due to the loop current of $J{\rm d}x{\rm d}z$ is given by $S(x)J{\rm d}x{\rm d}z$, where we have $S(x) = 2x[x + (l - w)/2]$. Therefore, the magnetic moment of a filament is given by $\int\int S(x)J{\rm d}x{\rm d}z$. If the number of filaments is $n_{\rm f}$, the

total magnetic moment of the tape specimen is given by

$$m = n_{\mathrm{f}} \int \int S(x) J \mathrm{d}x \mathrm{d}z = \frac{n_{\mathrm{f}} w^2 (3l - w) dJ}{12}. \tag{A.1}$$

From this equaton, we have

$$J = \frac{12m}{n_{\mathrm{f}} w^2 (3l - w) d}. \tag{A.2}$$

Thus, J can be estimated from the observed magnetic moment.

If the magnetic moment by a current flowing in the closed loop C is given by $m_{\mathrm{s}}(x)$, the magnetic flux through C is given by

$$\Phi(x) = B_{\mathrm{e}} S(x) + \frac{\mu_0 m_{\mathrm{s}}(x)}{d}. \tag{A.3}$$

From the relationship of $m = n_{\mathrm{f}} m_{\mathrm{s}}(w/2)$, the above equation is written as

$$\Phi(w/2) = wlB_{\mathrm{e}} + \frac{\mu_0 m}{n_{\mathrm{f}} d}. \tag{A.4}$$

Using a law of electromagnetic induction, the electric field inside the filament is obtained as

$$E(x) = -\frac{1}{4[2x + (l - w)/2]} \cdot \frac{\mathrm{d}\Phi(x)}{\mathrm{d}t}. \tag{A.5}$$

Therefore, from Eqs. (A.4) and (A.5), we have the electric field at the edge of the filament:

$$E(w/2) = -\frac{\mu_0}{2df(l + w)} \cdot \frac{\mathrm{d}m}{\mathrm{d}t}. \tag{A.6}$$

Thus, the E-J can be estimated from the observed magnetic moment m and its relaxation $\mathrm{d}m/\mathrm{d}t$using Eqs. (A.2) and (A.6). The current density corresponds to the mean value inside the filament, and the electric field corresponds to the maximum value at the edge of the filament.

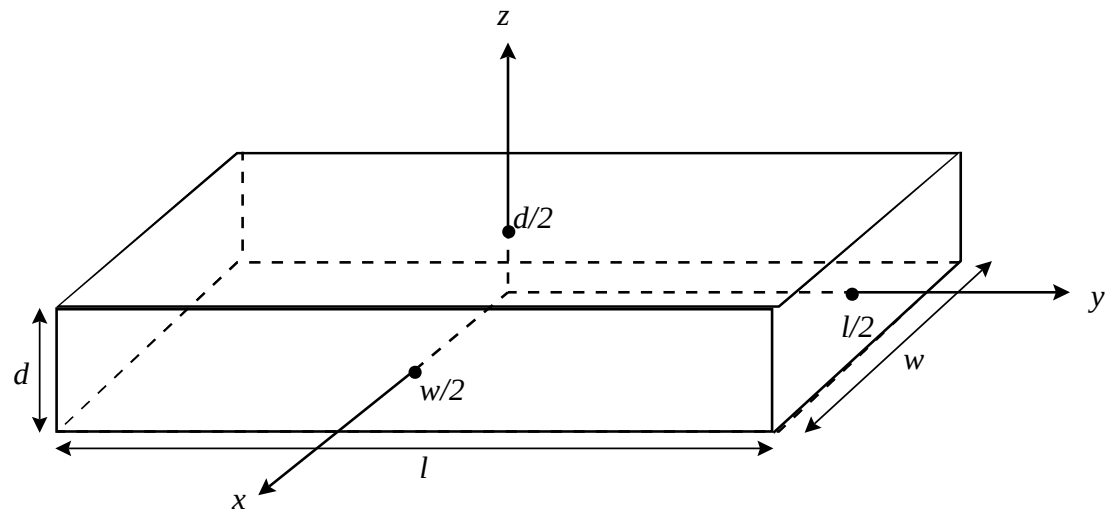

Fig. A.1. Rectangular superconducting filament.

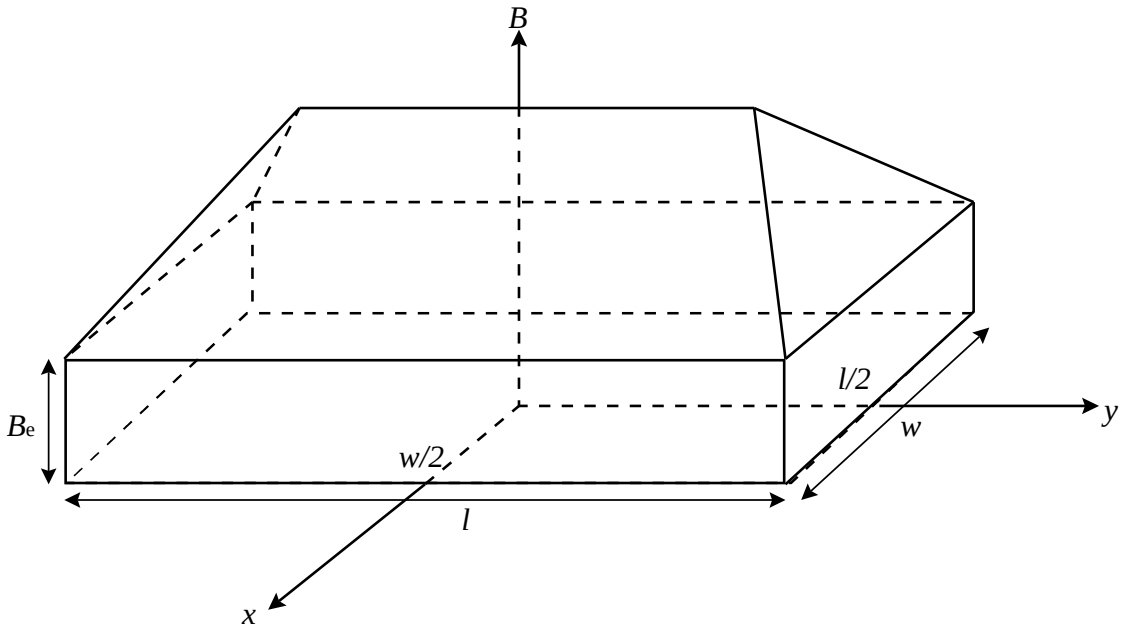

Fig. A.2. Flux distribution in the critical state in the filament after a magnetic field is decreased.

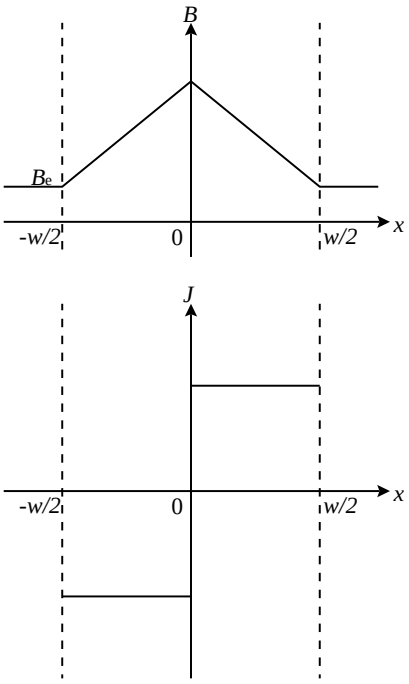

Fig. A.3. Flux distribution (top) and current distribution (bottom) along the direction of width.

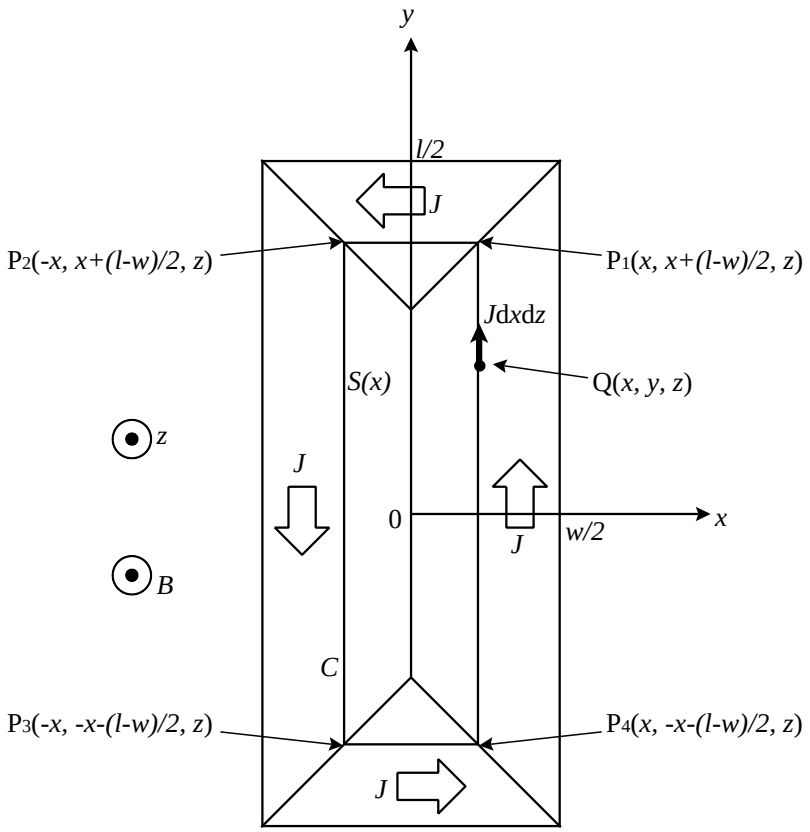

Fig. A.4. The current inside a plane parallel to a x-y plane.

Acknowledgments

The author would like to acknowledge profoundly Prof. T. Matsushita for giving a great number of the fruitful lectures, the leads and the advice for the performance of this study. The author would like to acknowledge profoundly Dr. E. S. Otabe for cooperating for the production of this paper and the experimental environment, and for giving the lectures and the leads. The author would like to thank Mr. R. Okamura who supported the experiment and the analysis in this study.

References

1) K. Yamafuji, T. Fujiyoshi, K. Toko and T. Matsushita: Physica C **159** (1989) 743.

2) T.Hasegawa,Y.Hikichi,T.Koizumi,A.Imai,H.Kumakura,H.Kitaguchi and K.Togano:IEEE Trans. Appl. Supercond. **7** (1997) 1703.

3) T.Hasegawa,Y.hikichi,H.Kumakura,H.Kitaguchi and K.Togano:Jpn. J. Appl. Phys. **34** (1995) 1638.

4) J.Kase,N.Irisawa,T.Morimoto,K.Togano,H.Kumakura,D.R.Dietderich and H.Maeda:Appl. Phys. Lett. **56** (1990) 970.

5) T. Matsushita: "On the Flux Bundle Size in Weakly Pinned Superconductors", Physica C **217** (1993) 461.

6) Y. Mawatari, A. Sawa, H. Obara, M. Umeda, H. Yamasaki : Phys. Rev. Lett. **70** (1997) 2300.

7) T. Nakamura, T. Kiss, Y. Hanayama, T. Matsushita, K. Funaki, M. Takeo, F. Irie, Advances in Superconductivity X (Springer-Verlag, Tokyo) (1998) 581.

8) T. Kodama : The graduate thesis, Kyshu Institute of Tecnology (1999).

9) M. P. A. Fisher : Phys. Rev. Lett. **62** (1989) 1416.

10) R. H. Koch, V. Foglietti, W. J. Gallagher, G.Koern, A. Grupta and M. P. A. Fisher : Phys. Rev. Lett. **63** (1989) 1511.

11) R. H. Koch, V. Foglietti and M. P. A. Fisher : Phys. Rev. Lett. **64** (1990) 2586.

12) T. Matsushita and T. Kiss: Thermal depinning of flux lines in superconductors. Physica C **315** (1999) 12.

13) Y. Mawatari, H. Yamasaki, S. Kosaka: IEEE Trans. Appl. Supercond. **5** (1995) 1305.

14) T. Matsushita , T. Tohgoh and N. Ihara: Effects of inhomogeneous flux pining strength and flux flow on scaling of current-voltage characteristics in high-temperature superconductors. Physica C **259** (1996) 321-325

15) T. Kiss, S. Nishimura, M. Inoue, H. Okamoto, M. kanazawa, Y. Sumiyoshi, to be published in proceeding of ICMC 2001.

16) Magnetic Property Mesurement System, QUANTUM DESIGN Ltd.

17) T. Matsushita, T. Tohdoh and N. Ihara: "Effects of Inhomogeneous Flux Pinning Strength and Flux Flow on Scaling of Current-Voltage Characteristics in High-Temperature Superconductors", Physica C **259** (1996) 321.

18) M. V. Feigel'man, V. B. Geshkenbein, A. I. Larkin and V. M. Vinokur: "Theory of Collective Flux Creep", Phys. Rev. Lett. **63** (1989) 2303.

19) M. P. A Fisher: "Vortex-Glass Superconductivity: A Possible New Phase in Bulk High T_c Oxides", Phys. Rev. Lett. **62** (1989) 1415.

20) D. S. Fisher, M. P. A. Fisher and D. A. Huse: "Thermal Fluctuations, Quenched Disorder, Phase Transitions, and Transport in Type-II Superconductors", Phys. Rev. B **43** (1991) 130.

21) T. Matsushita: Flux Pinning and Electromagnetic Phenomena (Sangyou Tosyo) p. 397.